Universidad Autónoma del Estado de México

Facultad de Ciencias

Estudio Analítico y numérico de la métrica no homogénea LTB con fuentes de energía momento generales. .

TESIS

que para obtener el grado de:

Maestria en Ciencias

(Física)

PRESENTA:

Lic. Roberto Carlos Blanquet-Jaramillo

:

Asesor: Dr. Máximo Agüero Granados (UAEM)

Co-asesor: Dr. Germán Izquierdo (UAEM)

Asesor-externo: Dr. Roberto A. Sussman (UNAM)

Toluca, Estado de México Junio, 2022

Capítulo 2

Resumen

El estudio del proceso de formación de estructura en el Universo es de vital importancia para la Cosmología y la Relatividad General. En este trabajo consideraremos fuentes de campo gravitacional que no tienen una distribución homogénea con simetría esférica. Por lo tanto, los potenciales que esperamos obtener van a ser no homogéneos y simétricamente esféricos. En particular, consideraremos dos fuentes de campo (materia oscura fría y energía oscura que admite presiones anisotrópicas) y lograremos reducir las ecuaciones de campo de Einstein a un sistema dinámico que consiste en ecuaciones de evolución que se pueden convertir en un sistema de ecuaciones diferenciales ordinarias de primer orden autónomas y vínculos algebraicos, los cuales contienen la información sobre las desviaciones respecto de la métrica con simetría esférica y homogénea. Las ecuaciones de evolución para las perturbaciones determinarán la dinámica de las estructuras que se formen, con su ubicación espacial especificada por las condiciones iniciales estándar del Universo temprano.

Capítulo 3

Protocolo aprobado y registrado.

3.1. Antecedentes

Toda teoría sobre la evolución del Universo y la formación de estructura deben satisfacer una gran cantidad de observaciones. Actualmente disponemos de muchas observaciones cosmológicas de alta calidad y precisión. Las observaciones cosmológicas sugieren que las fuentes de energía—materia cósmicas son predominantemente oscuras. Por ejemplo, la materia oscura fría (Cold dark matter, CDM) que se aglomera entorno a los halos galácticos forma aproximadamente es 27 % de la densidad total del Universo (densidad critica). La energía oscura está asociada a la expansión acelerada cósmica que sugieren las observaciones y consiste en aproximadamente un 68 % de la densidad crítica. La materia visible que se encuentra en estrellas, agujeros negros, planetas, galaxias, etc., asciende a sólo el 5 % de la densidad critica. Dicha densidad critica es una medida de densidad que podemos formar con constantes fundamentales y la medición de la expansión cósmica a través del factor de Hubble. Una gran cantidad de observaciones independientes sugieren que la mejor descripción de la evolución del Universo a gran escala (una granulación de 150

Mpc, que es una vigésima parte de la distancia del Universo observable). Esta descripción a gran escala está dada por el llamado modelo de constante cosmológica. En el modelo de constante cosmológica la dinámica cósmica a grandes escalas se describe mediante perturbaciones lineales sobre un fondo homogéneo e isotrópico el cual se llama Lambda-CDM cuyas fuentes son las fuentes mencionadas anteriormente, es decir, la materia oscura fría y la materia visible siendo la energía oscura descrita a través de la constante cosmológica. Para describir la energía oscura es necesario considerar un fluido con presión negativa, usualmente expresamos la presión como proporcional a la densidad ($p = w\rho$) donde en este caso la constante de proporcionalidad debe ser negativa ($w < 0$). La forma más simple es la que se usa en el modelo de constante cosmológica en la cual ($p = -\rho$, o $w = -1$) que corresponde. Sin embargo hay otras posibilidades, por ejemplo, se puede considerar una energía oscura dinámica ($w < -1/3$ y dependiente del tiempo). Desafortunadamente estos modelos tienen problemas de ajuste fino al tratar de adecuarse a la fenomenología del universo temprano [1].

Las fluctuaciones en la densidad de la CDM son las que dan lugar a la formación de estructura (galaxias, clústers, etc.) y es posible obtener límites a los modelos de energía oscura a través de los datos observados. Las fluctuaciones de densidad han sido estudiadas en la literatura a orden perturbativo lineal [2,3]. Para estudiar la formación de estructura en est trabajo pensamos utilizar ecuaciones exactas de las ecuaciones de Einstein. Estas ecuaciones son un sistema acoplado de diez ecuaciones diferenciales parciales de segundo orden muy difíciles de resolver. Nuestro propósito es utilizar métricas y distribuciones de energía-materia lo suficientemente idealizadas para poder obtener soluciones analíticas de las ecuaciones de Einstein pero que no sean soluciones tan sencillas que supongan

soluciones triviales. Una familia de métricas que cumple esos requisitos son las métricas Lemaître-Tolman-Bondi (LTB)

$$ds^2 = -dt^2 + \frac{R'^2 dr^2}{1+E} + R^2[d\theta^2 + \sin^2\theta d\phi^2], \tag{3.1}$$

donde $R = R(ct, r)$, $R' = \partial R/\partial r$ y $E = E(r)$. El tensor energía—momento para un fluido con presión anisotrópica que utilizaremos en las ecuaciones de Einstein es

$$T^{ab} = \rho u^a u^b + p h^{ab} + \Pi^{ab}, \tag{3.2}$$

donde $\rho = \rho(ct, r)$ y $p = p(ct, r)$ son respectivamente densidad y presión del fluido fuente (o mezclas de fluidos) que llena el universo, u^a es la cuadrivelocidad del elemento de fluido y h^{ab} es la métrica inducida sobre la hypersuperficie a tiempo constante y Π^{ab} es la presión anisotrópica de la fuente. Definiendo los escalares cuasi-locales [4], a partir de las funciones escalares ρ, p, E y R, y con las ecuaciones de campo $G^{ab} = \kappa T^{ab}$ ($\kappa = 8\pi G$) se obtienen las siguientes ecuaciones de evolución

$$\dot{\rho}_q = -3\left[1+w\right]\rho_q \mathcal{H}_q, \tag{3.3}$$

$$\dot{\mathcal{H}}_q = -\mathcal{H}_q^2 - \frac{\kappa}{6}\left[1+3w\right]\rho_q, \tag{3.4}$$

$$\dot{\delta}^{(\rho)} = 3\mathcal{H}_q\left[\left(\delta^{(\rho)} - \delta^{(p)}\right)w - \left(1 + w + \delta^{(\rho)}\right)\delta^{(\mathcal{H})}\right], \tag{3.5}$$

$$\begin{aligned}\dot{\delta}^{(\mathcal{H})} = & -\mathcal{H}_q\left(1+\delta^{(\mathcal{H})}\right)\delta^{(\mathcal{H})} \\ & + \frac{\kappa\rho_q}{6\mathcal{H}_q}\left[\delta^{(\mathcal{H})} - \delta^{(\rho)} + 3w\left(\delta^{(\mathcal{H})} - \delta^{(p)}\right)\right],\end{aligned} \tag{3.6}$$

donde $\mathcal{H}_q = \dot{R}/R$, $\mathcal{K}_q = -E/R^2$ y $\dot{\mathcal{K}}_q/\mathcal{K}_q = -2\mathcal{H}_q$. Dichas ecuaciones permiten interpretar la función $\mathcal{H}_q$ como el factor de Hubble de la métrica homogénea y la función $\mathcal{K}_q$ como un término de curvatura. Aunque ambas tienen dependencia en la coordenada r, la densidad y presión cuasi-locales están relacionadas a través de la ecuación de conservación de energía

que es análoga a la ecuación de la métrica homogénea a pesar de que densidad y presión cuasi-locales también dependen de la coordenada r. La desviación de la homogeneidad de la métrica viene dada por unas funciones que llamamos $\delta^{\mathcal{H}}$, $\delta^{\mathcal{K}}$, δ^{ρ} y δ^{p} y que contienen la dependencia de las funciones cuasi-locales respecto de r. Las ecuaciones de Einstein nos dan unas ecuaciones de evolución para las funciones δ que debemos completar con una definición de la densidad y presión del fluido considerados (o en algunos casos con una ecuación de estado que relacione a ambas).

El trabajo que proponemos va a ser una generalización a los modelos utilizados en el trabajo de Licenciatura [4]. En este trabajo consideraremos la métrica LTB con una descripción de ambos fluidos más general que admita otro tipo de interacciones y ecuaciones de estado más generales. En dicho trabajo podíamos describir la CDM como un fluido no homogéneo sin presión y a la energía oscura como un fluido con ecuación de estado barotrópica que interactuaban con un tipo de interacción sencilla. Los modelos de espacio–tiempos con métricas no homogéneas permiten una descripción completa de las perturbaciones en la densidad y es posible que a gran escala tiendan a comportarse como la métrica homogénea Friedman-Lemaître-Robertson-Walker (FLRW). Un ejemplo de este tipo es la métrica LTB que es esféricamente simétrica, con lo cual es posible describir fluctuaciones que presentes simetría esférica. A menudo esta métrica se utiliza para obtener soluciones locales que puedan describir un gas en una parte del Universo (nebulosas) y/o la formación de estructura en el Universo temprano donde todavía se dan flujos de energía locales.

Existe una conexión con la teoría de las perturbaciones cosmológica y las fluctuaciones de los escalares cuasi-locales ya que representan una generalización analítica e invariantes

de las funciones covariantes de las perturbaciones cosmológicas [7,8]. Es muy poco conocido que la métrica LTB con tensores energía–momento con presión distinta de cero en un marco comóvil. Para un fluido perfecto la presión debe ser uniforme (gradientes de presión cero), lo que permite interpretar la fuente como una mezcla compuesta por un fluido de densidad de energía oscura homogéneo que interactúa con polvo no homogéneo que representa la materia oscura fría (ver [6, 9]). La métrica LTB con una fuente de energía de tipo polvo (CDM) y una segunda fuente en forma de constante cosmológica ofrece una generalización sencilla pero útil del modelo Lambda-CDM [5, 6]. Para fluidos con presión anisotrópica, admiten gradientes de presión no triviales, lo que conduce a una descripción similar en términos de escalares cuasi-locales y sus fluctuaciones como en los modelos LTB de polvo. Para los fluidos anisotrópicos, la anisotropía de la presión puede estar relacionada con la fluctuación del escalar cuasi-local asociado con la presión isotrópica. Dado que es posible establecer mezclas de fluidos y una amplia variedad de ecuaciones de estado son admisibles, se han utilizado métricas LTB con estas fuentes para modelar mezclas no homogéneas de energía oscura y materia oscura fría [6,9]. En [4], se estudia una métrica LTB esféricamente simétrica y no homogénea que contiene una mezcla de materia oscura fría no relativista y energía oscura acoplada con ecuación de estado constante, con un término de acoplamiento proporcional a la densidad de materia oscura fría. En [10], examinamos la evolución de una mezcla no homogénea de materia oscura fría no relativista sin presión, acoplada a la energía oscura caracterizada por la ecuación de estado $w < -1/3$, con el término de interacción proporcional a la densidad de energía oscura.

3.2. Justificación.

Dado que no se puede observar la materia ni la energía oscuras directamente, los límites teóricos de los parámetros de los modelos y las observaciones indirectas son la única información de su naturaleza que se puede obtener. Una de las observaciones más importantes que hoy día tenemos está relacionada con la cantidad, la distribución y el tamaño de las galaxias y clústers de galaxias existentes en el Universo. Dado que esas estructuras se han formado siguiendo una dinámica muy dependiente del modelo cosmológico considerado, esos datos permiten validar y dar límites a los modelos de universo existentes. El conocimiento de los procesos de formación de estructura es muy importante para poder obtener dichos límites. En nuestro trabajo estudiaremos dichos procesos como soluciones exactas de las ecuaciones de Einstein.

3.3. Objetivos generales.

Generalizar los modelos LTB de [3] para describir fuentes con presiones e interacciones entre dichas fuentes más generales. Obtener ecuaciones de evolución como un sistema dinámico que permitan comprender como se desvían estas métricas de las métricas FLRW mediante los escalares cuasi-locales. Estudiar los sistemas dinámicos que forman las ecuaciones de evolución.

3.4. Objetivos espesíficos.

Considerar dos fuentes en la métrica LTB: CDM con presión nula y una fuente de energía oscura con presión negativa general . Resolver las ecuaciones para ejemplos con-

cretos y perfiles de masa/energía y curvatura iniciales determinados, que nos permitan hallar límites concretos en esos modelos. Calcular el tiempo de colapso de una esféra en la métrica LTB.

3.5. Planteamiento.

En este trabajo se resolverá por medio de métodos numéricos el sistema dinámico de las ecuaciones de evolución del modelo de universo LTB con dos fuentes (CDM y energía oscura)para diferentes condiciones iniciales: perfiles de materia oscura, modelos de energía oscura, curvatura, etc. Se hará especial énfasis en los modelos de formación de estructura.

3.6. Metodología.

Se realizará la revisión bibliográfica necesaria para comprender la parte física y matemática del problema y así deducir las ecuaciones de evolución. Generar programas en Maple 13 para hallar soluciones numéricas en diferentes escenarios. Generar gráficas con los límites teóricos obtenidos. Comparar los resultados a los límites obtenidos con los reportados en otros trabajos (y/o artículos).

3.7. Apoyo e infraestructura.

Contamos con equipo de cómputo que posee acceso a Internet. El material bibliográfico lo estamos adquiriendo en forma constante y actualizada para el desarrollo del trabajo. Usaremos Maple 13 para la solución de las ecuaciones y la presentación de los resultados.

3.8. Actividades.

Actividad	Semestre 1	Semestre 2	Semestre 3	Semestre 4
Revisión bibliográfica.	X	X	X	X
Estudio de la métrica LTB	X	X	X	X
Generación del código			X	X
Simulación y análisis de los resultados			X	X
Elaboración de Artículo				X
Redacción de la Tesis			X	X
Trámites y defensa de Tesis				X

3.9. Trayectoria académica.

Se proponen los siguientes cursos, según el plan de Maestría en Ciencias: Curso en Ciencias I: Mecánica Cuántica. Curso en Ciencias II: Mecánica Clásica. Curso en Ciencias II: Electrodinámica. Curso en Ciencias VI: Física Estadistica. Curso en Ciencias V: Temas selectos. Curso en Ciencias VI: Temas selectos.

3.10. Productos entregables.

1.-Artículo de investigación enviado a una revista perteneciente a JCR con índice de impacto. 2.-Se presentarán resultados en un congreso nacional o internacional. 3.-Obtención del grado de Maestro en Ciencias.

Capítulo 4

Carta de aceptación y artículo

Carta de aceptación en la revista especializada Modern Physics Letters A:

Gmail **German Izquierdo <german.izquierdo@gmail.com>**

Your Submission: MPLA-D-21-00423R1

Mod. Phys. Lett. A (MPLA) <em@editorialmanager.com> 6 de junio de 2022, 1:34
Responder a: "Mod. Phys. Lett. A (MPLA)" <mpla@wspc.com>
Para: German Izquierdo <german.izquierdo@gmail.com>

Ref.: Ms. No. MPLA-D-21-00423R1
Evolution equations dynamical system of the Lemaître--Tolman--Bondi metric containing coupled dark energy.
Modern Physics Letters A

Dear Dr. Izquierdo,

I am pleased to inform you that your work has now been accepted for publication in Modern Physics Letters A (MPLA).

It was accepted on Jun 06, 2022.

Comments from the Editor and Reviewer can be found below.

--- ---
We would like to take the opportunity to re-iterate that in line with models adopted by other physics journals, MPLA offers its authors an option whereby their accepted manuscripts will be available barrier-free and open access (OA) on publication. Open access articles are on fast track publication, and your article will be published online within 7 working days upon receiving your confirmation for OA.*

Should you wish to opt for the open access option, please refer to our OA options for MPLA/IJMPA at https://www.worldscientific.com/mpla/openaccess. Kindly inform us of your choice at mpla@wspc.com at your earliest convenience. The page includes information regarding special arrangements and subsidies World Scientific has with select institutions and organisations for publishing in OA. For inquiries on possible Open Access publication funding from your institution, please contact us at openaccess@wspc.com.

Why Open Access?

MPLA is in full compliance with the latest open access mandates so authors can ensure their research is freely available online, freely redistributed and reused under the terms of Creative Commons Attribution license (CC BY 4.0 https://creativecommons.org/licenses/by/4.0/). Benefits of open access include immediate and unrestricted access to the final published paper; higher visibility & possibility of being cited; copyright retained by author.

*Open Access option: *the article will be published within 7 working days under the condition that the authors approve the proof within one working day.*

If you choose non-Open Access for your article, please be informed of the transfer of copyright as stated on MPLA's submission guidelines: "Once a paper is accepted, authors are assumed to have transferred the copyright of the paper to World Scientific."
--- ---

We thank you for choosing to publish with us and we look forward to receiving your next submission.

Yours sincerely,
MPLA Editors
WSPC Journal Office
Modern Physics Letters A

Comments from the Editor and Reviewer:

Reviewer #1: I would like to thank the authors for their thoughtful and convincing responses to my comments. The changes look good, and the presentation of the manuscript is better than before. I am pleased to recommend the

revised version for publication.

Reviewer #2: The authors have introduced an important number of changes to their original manuscript in response the previous reports of the referees. In my opinion, the present version addresses to satisfaction the issues that were pointed out to the authors. Therefore I believe the manuscript now deserves publication in the Modern Physics Letters A, and hence I recommend it.

Versión actualizada del artículo en los arXiv:

Evolution equations dynamical system of the Lemaître–Tolman–Bondi metric containing coupled dark energy.

Roberto C. Blanquet-Jaramillo[†], Roberto A. Sussman[‡], Máximo A. Agüero Granados[†], German Izquierdo[†]

[†] Facultad de Ciencias, Universidad Autónoma del Estado de México, Toluca 5000, Instituto literario 100, Edo. Mex.,México.

[‡] Instituto de Ciencias Nucleares, Universidad Nacional Autónoma de México (ICN-UNAM),A. P. 70–543, 04510 México D. F., México.

E-mail: gizquierdos@uaemex.mx

Abstract. We consider inhomogeneous spherically symmetric models based on the Lemaître-Tolman-Bondi (LTB) metric, assuming as its source an interactive mixture of ordinary baryonic matter, cold dark matter and dark energy with a coupling term proportional to the addition of energy densities of both dark fluids. We reduce Einstein's field equations to a first order 7-dimensional autonomous dynamical system of evolution equations and algebraic constraints. We study in detail the evolution of the energy density and spatial curvature profiles along the phase space by means of two subspace projections: a three-dimensional projection associated with the solutions of the Friedman-Lemaître-Robertson-Walker metric (invariant subspace) and a four-dimensional projection describing the evolution of the inhomogeneous fluctuations. We also classify and study the critical points of the system in comparison with previous work on similar sources, as well as solving numerically the equations for initial energy density and curvature profiles that lead to a spherical bounce whose collapsing time we estimate appropriately.

PACS numbers: 98.80.-k, 04.20.-q, 95.36.+x, 95.35.+d

1. Introduction.

Cosmological observations indicate that the Universe contains three primary matter-energy sources: baryonic matter, cold dark matter (CDM) and dark energy (DE), respectively making 5 %, 27 % and 68 % of the total content [1]. Observational data strongly support the ΛCDM model in which dark energy is empirically described in our cosmic time by a cosmological constant equivalent to a source with pressure $p = -\rho$. However, this empiric model and other non-interactive dynamic dark energy models present a problematic "coincidence problem" that can be alleviated once we assume a non-trivial interaction between the dark sources (since it is safe to assume that non-gravitational interaction between the latter and visible matter must be very weak) [2]. Several coupled models have been suggested and studied in detail (see examples in [3]).

Observational data also supports a Friedman–Lemaître–Robertson–Walker (FLRW) background metric with energy density linear perturbations [1, 5, 6], and observed local structure described by non–linear dynamics (whether Newtonian or relativistic) [4]. Given the large amount of available DE and CDM models, it is necessary to contrast their predictions against observational data [7, 8, 10, 11].

In order to study the structure formation, non–linear Newtonian dynamics is generally used (see review [12]), as at larger scales (subhorizon) CDM can be well approximated by a pressure–less dust fluid, while a cosmological constant can play the role of the DE source. On the other hand, General Relativity is necessary to describe a more general DE source with a different pressure (whether interacting of not with the CDM, [13]). While numerical simulation involving continuous modeling or N–body solutions can address the problem, inhomogeneous metrics that are exact solutions of Einstein's equations offer a idealized but interesting approach to the problem as they provide some analytical/physical results that complement the numerical work.

An example of the latter is the spherically symmetric Lemaître–Tolman–Bondi (LTB) metric. LTB metrics are typically associated in the astrophysical and cosmological literature with a pure dust source [14], with/without cosmological constant [15, 16, 17, 18]. However, the exact solutions provided by it are also compatible with nonzero pressures (something that it is often not known). In particular, it is possible to define a class of "quasi–local scalars" (QL scalars [19, 20, 21, 22]) that permit a clear, yet complete, description of the theoretical properties and evolution of sources with zero and nonzero pressure in terms of averages of standard covariant scalars satisfying FLRW dynamics, and the deviation from a FLRW background described by fluctuations with respect to the QL scalars [21], all this with both the QL scalars and fluctuations being coordinate independent covariant quantities [22]. The QL scalars and their fluctuations transform Einstein's field equations for LTB models into evolution equations that can be set up as a self-consistent dynamical system (e.g., as has been done for dust models without and with a cosmological constant term, in [23, 24] and [25] respectively). Connection of the LTB inhomogeneous metric with the FLRW linear perturbation theory is straightforward as a set of delta functions is defined (as the local scalar function divided by the corresponding QL quantity minus 1) that can be put in correspondence with cosmological perturbations in the isochronous gauge [24, 26].

LTB metrics are compatible with mixtures of an homogeneous DE fluid and an inhomogeneous CDM dust [27], but also with mixtures of dark fluids with anisotropic pressures [28, 29] by means of the QL scalars associated with the isotropic pressure.

We have studied previously LTB metric models by means of the QL formalism [28, 23, 25, 26, 30, 31, 32], more recently considering as sources mixtures of non-relativistic CDM, described as dust, coupled to DE described as a dark fluid with constant equation of state $w < -1/3$. In [30] we assumed the coupling term to be proportional to CDM energy density, while in [31] it was proportional to the DE density. In the present article, we generalize the previous results by considering a coupling term proportional to the addition of both dark sources energy densities and considering an additional pressure–less uncoupled baryonic matter source. We study the 7–dimension dynamical system of the evolution equations and we classify the corresponding critical points. This analytical study give us an invaluable analytical information on the evolution of both QL scalars and perturbations that can help to understand and improve the numerical solutions. We also compute the evolution of a given set of initial conditions in order to illustrate the analytical findings. The initial profile chosen shows an scenario describing the outset of spherical collapse that could be interpreted as an idealized spherically symmetric structure formation example.

The section by section disposition of the present article come next. In section 2 we describe the QL formalism and the corresponding differential equations for the LTB metric considered. In section 3, we find the critical points in terms of the free parameters (FPs). In section 4, we study the necessary conditions to avoid singularities and set the initial profiles to illustrate an structure formation scenario. In section 5, we compare the results found in this work with other coupling terms in the literature. Finally, in section 6, we outline our findings. In this manuscript, we make use of natural units, $c = 1$.

2. LTB spacetimes, Q–scalar variables and coupled dark energy model

The LTB metrics describe inhomogeneous spherically symmetric solutions that represent exact local density perturbations tending asymptotically to an homogeneous FLRW metric. The models generalize the Newtonian spherically-symetric collapse in order to describe the evolution of non–relativistic spherical dust perturbations that start from a linear regime in the early Universe towards a fully non-linear regime just before virialization. This description allow us to consider a CDM and DE sources that provides a plain but useful generalization of the Λ-CDM model [25, 30, 31]. The LTB metric can be written as

$$ds^2 = -dt^2 + \frac{R'^2\, dr^2}{1-K} + R^2[d\theta^2 + \sin^2\theta\, d\phi^2], \tag{1}$$

where $R = R(t,r)$ is a general function of the time t and the radius coordinate r, $' = \partial/\partial r$, and $K = K(r)$ is a function related to the spatial curvature of the metric.

In order to model sources with non-trivial pressure we consider the most general energy–momentum tensor of the fluid compatible with the metric (1) in a comoving frame with $u^a = \delta^a_t$

$$T^{ab} = \rho\, u^a u^b + p\, h^{ab} + \Pi^{ab}, \tag{2}$$

where $\rho = \rho(t,r)$ y $p = p(t,r)$ are respectively the energy density and isotropic pressure and $\Pi^a_b = \mathcal{P}(t,r) \times \mathrm{diag}[0,-2,1,1]$ is the anisotropic pressure tensor of the fluid (a spacelike symmetric traceless tensor), while $h^{ab} = g^{ab} + u^a u^b$ is the metric induced on the hypersurface at a constant time t. Considering the fluid as a mixture of non-relativistic baryonic matter, together with non-relativistic CDM coupled to DE, the

total energy density and isotropic pressure are

$$\begin{aligned}\rho &= \rho_b + \rho_m + \rho_e,\\ p &= p_b + p_m + p_e,\end{aligned} \tag{3}$$

where ρ_b, p_b, ρ_m, p_m and ρ_e, p_e are respectively the energy density and pressure of baryonic matter, CDM and DE mixture components. The conserved total energy–momentum tensor ($\nabla_b T^{ab} = 0$) can be decomposed as

$$T^{ab} = T^{ab}_{\mathrm{b}} + T^{ab}_{\mathrm{m}} + T^{ab}_{\mathrm{e}}. \tag{4}$$

with an interaction between CDM and DE described by energy-momentum flux (coupling current) between them as

$$j^a = \nabla_b T^{ab}_{(m)} = -\nabla_b T^{ab}_{(e)}. \tag{5}$$

Given the symmetry of the metric (1), $h_{ca} j^a = 0$ holds as the current must be parallel to the 4–velocity. Then, $j_a = J u_a$ with

$$J = u_a \nabla_b T^{ab}_m = -u_a \nabla_b T^{ab}_e, \tag{6}$$

Our LTB model, then, has seven local scalar fields dependent of the fluid surces whose evolution has to be solved: $A(t,r) = \rho_b$, ρ_m, ρ_e, p_b, p_m, p_e, and J. Following the quasi–local scalars (QL scalars) description of the LTB metrics [30, 31, 28, 29], QL scalar A_q and fluctuation δ^A are defined for every A as

$$A_q = \frac{\int_{x=0}^{x=r} A\, R^2 R' dx}{\int_{x=0}^{x=r} R^2 R' dx}, \qquad \delta^A = \frac{A - A_q}{A_q} = \frac{A'_q/A_q}{3R'/R}, \tag{7}$$

where $x = 0$ is a symmetry centre of the metric and $R(t,0) = \dot{R}(t,0) = 0$, with $\dot{} = \partial/\partial t$, and $\dot{R} = u^a \nabla_a R$. The QL pressures of the sources are related to the anisotropic pressures as follows

$$\begin{aligned} p_{bq} &= p_b - 2\mathcal{P}_b, \quad \delta^p_{(b)} = 2\mathcal{P}^{(b)},\\ p_{mq} &= p_m - 2\mathcal{P}^{(m)} \quad \delta^p_{(m)} = 2\mathcal{P}^{(m)},\\ p_{eq} &= p_e - 2\mathcal{P}^{(e)}, \quad \delta^p_{(e)} = 2\mathcal{P}^{(e)}. \end{aligned} \tag{8}$$

Additionally, there are two covariant scalars associated to the metric (1): the Hubble expansion scalar $\mathcal{H} = (1/3)\nabla_a u^a = (R^2R')\dot{}/(R^2R')$, and the spatial curvature $\mathcal{K} = (1/6)^3\mathcal{R} = 2(KR)'/(R^2R')$, where the later is related to the Ricci scalar ${}^3\mathcal{R}$ of constant t hypersurfaces with induced metric h_{ab}. The corresponding QL scalars read

$$\mathcal{H}_q = \frac{\dot{R}}{R}, \qquad \mathcal{K}_q = \frac{K}{R^2}. \tag{9}$$

The local interaction term J is also scalar and defines a QL interaction J_q and a corresponding delta ($J = J_q(1 + \delta^{(J)})$). In this work, we consider that J_q depends on the rest of QL scalars and will be defined later. In order to obtain the evolution equations of the model, we need to consider the following equations of state (EOS) for the different sources

$$\text{baryonic matter (dust):} \qquad p_b = 0 \quad \Rightarrow \quad \delta^p_{(b)} = 0 \tag{10}$$

$$\text{CDM (dust):} \qquad p_m = 0 \quad \Rightarrow \quad \delta^p_{(m)} = 0, \tag{11}$$

$$\text{DE (barotropic fluid):} \qquad p_e = w\rho_e \quad \Rightarrow \quad \delta^p_{(e)} = \delta^\rho_{(e)}, \tag{12}$$

where we have assumed that w is a constant. According to equations (10-12), the DE source is the only one that contributes to the anisotropic pressure: $\mathcal{P} = \mathcal{P}^{(e)} = \delta^{p}_{(e)}/3$. As in [30, 31, 28, 29], the evolution equations are

$$\dot{\mathcal{H}}_q = -\mathcal{H}_q^2 - \frac{\kappa}{6}\left[\rho_{mq} + (1+3\,w\,)\rho_{eq} + \rho_{bq}\right] \tag{13a}$$

$$\dot{\rho}_{bq} = -3\mathcal{H}_q\,\rho_{bq}, \tag{13b}$$

$$\dot{\rho}_{mq} = -3\mathcal{H}_q\,\rho_{mq} + J_q, \tag{13c}$$

$$\dot{\rho}_{eq} = -3\mathcal{H}_q\,(1+w)\;\rho_{eq} - J_q, \tag{13d}$$

$$\begin{aligned}\dot{\delta}^{(\mathcal{H})} = &-\mathcal{H}_q\delta^{(\mathcal{H})}\left(1+3\delta^{(\mathcal{H})}\right) + \frac{\kappa}{6\mathcal{H}_q}\left[\rho_{mq}\,\left(\delta^{(\mathcal{H})}-\delta^{(m)}\right)\right.\\ &\left.+(1+3w)\rho_{eq}\,\left(\delta^{(\mathcal{H})}-\delta^{(e)}\right)+\rho_{bq}\,\left(\delta^{(\mathcal{H})}-\delta^{(b)}\right)\right],\end{aligned} \tag{13e}$$

$$\dot{\delta}^{(b)} = -3\mathcal{H}_q\,\delta^{(\mathcal{H})}\left[1+\delta^{(b)}\right], \tag{13f}$$

$$\dot{\delta}^{(m)} = -3\mathcal{H}_q\,\left(1+\delta^{(m)}\right)\delta^{(\mathcal{H})} + \frac{J_q}{\rho_{mq}}\left(\delta^{(J)}-\delta^{(m)}\right), \tag{13g}$$

$$\dot{\delta}^{(e)} = -3\mathcal{H}_q\,\left(1+w+\delta^{(e)}\right)\,\delta^{(\mathcal{H})} - \frac{J_q}{\rho_{eq}}\left(\delta^{(J)}-\delta^{(e)}\right). \tag{13h}$$

with the constraints

$$\mathcal{H}_q^2 = \frac{\kappa}{3}\left[\rho_{bq}+\rho_{mq}+\rho_{eq}\right] - \mathcal{K}_q, \tag{14}$$

$$2\mathcal{H}_q^2\delta^{(\mathcal{H})} = \frac{\kappa}{3}\left(\rho_{bq}\delta^{(b)}+\rho_{mq}\delta^{(m)}+\rho_{eq}\delta^{(e)}\right) - \mathcal{K}_q\delta^{(\kappa)}. \tag{15}$$

where $\kappa = 8\pi G$, (15) follows from (14) and (7), $\delta^{(\kappa)} = (\mathcal{K}-\mathcal{K}_q)/\mathcal{K}_q$. The evolution equations (13*a*–13*d*)and the constraint(14), at every comoving shell $r = r_i$, are similar to the corresponding FLRW evolution equations.

Also, in the limit $r \to \infty$, the LTB metric can be matched to a FLRW background as $\delta^{(b)}$, $\delta^{(m)}$, $\delta^{(e)}$, $\delta^{(\mathcal{H})}$, $\delta^{(J)}$ vanish, [19]. The differential equations system (13*a*–13*h*) depends on the FP w and the scalar J_q. In this work, the J_q considered is

$$J_q = 3\mathcal{H}_q\,\alpha\,\left(\rho_{mq}+\rho_{eq}\right) \tag{16}$$

$$\delta^{(J)} = \delta^{(\mathcal{H})} + \frac{\rho_{mq}\,\delta^{(m)}}{(\rho_{mq}+\rho_{eq})} + \frac{\rho_{eq}\,\delta^{(e)}}{(\rho_{mq}+\rho_{eq})}, \tag{17}$$

where α is a dimensionless coupling constant. This coupling term is considered in the literature (see [7, 8, 9, 34]) in the context of FLRW cosmology. It represents a generalization of the coupling terms used in [30, 31], $J_q = 3\mathcal{H}_q\alpha\rho_{mq}$ and $J_q = 3\mathcal{H}_q\alpha\rho_{eq}$, respectively. Given the evolution of the QL energy densities of CDM and DE (CDM dominating the early universe expansion, while DE dominates the late expansion), it is expected that the coupling (16) behaves as the coupling in [30] in the early universe and behaves as the coupling in [31] for the late expansion of the metric.

For $\alpha > 0$ and with the definition in (6), it is straightforward to conclude that energy density flows from the DE to the CDM. This coupled DE model have been studied in the frame of FLRW metrics in [5, 7, 10], where the energy density flux term (Q) is an homogeneous scalar that represents phenomenologically the microscopical interaction between the DE scalar field and the CDM particles.

2.1. QL scalars scaling laws

Metric (1) can be rewritten as

$$\mathrm{d}s^2 = -\mathrm{d}t^2 + L^2\left[\frac{\Gamma^2 {R_0'}^2 \mathrm{d}r^2}{1-\mathcal{K}_{q0}R_0^2} + R_0^2\left(\mathrm{d}\theta^2 + \sin^2\theta \mathrm{d}\phi^2\right)\right], \tag{18}$$

$$\Gamma = \frac{R'/R}{R_0'/R_0} = 1 + \frac{L'/L}{R_0'/R_0}, \tag{19}$$

where $L = L(t,r)$ is a generalization of the FLRW scale factor. Given the LTB metric invariance under radial coordinate rescaling, it is possible to specify the function $R_0(r)$ in order to define a physical radial coordinate $\mathfrak{R} = R_0(r)$, as $d\mathfrak{R} = R_0' dr$. We can set the Big Bang singularity at the instant for which $L(t,r) = 0$, while $\Gamma(t,r) = 0$ would define a shell crossing singularity [25].

Solving evolution equations (9), (13*a*), (13*b*),(13*c*) and (13*d*) with respect to L, we obtain the scaling laws for the QL scalars (equivalent to scaling laws of the analogous FLRW scalars),

$$\begin{aligned}
\mathcal{K}_q &= \mathcal{K}_{q0}L^{-2}, \quad \rho_{bq} = \rho_{bq0}L^{-3}, \\
\rho_{eq} &= \rho_{eq0}\left(aL^{\gamma_1} + (1-a)L^{\gamma_2}\right) + \rho_{mq0}b(-L^{\gamma_1} + L^{\gamma_2}), \\
\rho_{mq} &= \rho_{mq0}\left((1-a)L^{\gamma_1} + aL^{\gamma_2}\right) + \rho_{eq0}b(L^{\gamma_1} - L^{\gamma_2}),
\end{aligned} \tag{20}$$

where

$$\begin{aligned}
a &= \frac{1}{2} + \frac{2\alpha + w}{2w\Delta},\ b = -\frac{\alpha}{w\Delta}, \\
\gamma_1 &= -\frac{3}{2}(2 + w(1+\Delta)),\ \gamma_2 = -\frac{3}{2}(2 + w(1-\Delta)), \\
\Delta &= \sqrt{1 + 4(\alpha/w)}.
\end{aligned} \tag{21}$$

3. The non-dimensional evolution equations system

In order to transform (13*a*–13*h*) into a proper autonomous dynamical system associated with cosmological variables, it is necessary to define the following dimensionless energy density Ω functions

$$\Omega_b = \frac{\kappa}{3\mathcal{H}_q^2}\rho_{bq}, \qquad \Omega_m = \frac{\kappa}{3\mathcal{H}_q^2}\rho_{mq}, \qquad \Omega_e = \frac{\kappa}{3\mathcal{H}_q^2}\rho_{eq}. \tag{22}$$

whose evolution equations follow from (13*a*), (13*b*), (13*c*), and (13*d*) as

$$\frac{1}{\mathcal{H}_q}\dot{\Omega}_A = \frac{\kappa}{3\mathcal{H}_q^3}\dot{\rho}_{Aq} - \Omega_A\frac{\dot{\mathcal{H}}_q}{\mathcal{H}_q}, \tag{23}$$

with $A = b, m, e$. The constraints (14) and (15) in terms of the Ω functions are

$$\Omega_b + \Omega_m + \Omega_e + \Omega_{\mathcal{K}} = 1, \tag{24}$$

$$2\delta^{(\mathcal{H})} = \Omega_b\delta^{(b)} + \Omega_m\delta^{(m)} + \Omega_e\delta^{(e)} + \Omega_{\mathcal{K}}\delta^{(\kappa)}. \tag{25}$$

where $\Omega_{\mathcal{K}} = -\mathcal{K}_q/\mathcal{H}_q^2$. It is convenient to define for all comoving observers $r = r_i$ a dimensionless time coordinate $\xi(t,r)$ [25]

$$\frac{\partial}{\partial\xi} = \frac{1}{\mathcal{H}_q}\frac{\partial}{\partial t} = \frac{3}{\Theta_q}\frac{\partial}{\partial t}. \tag{26}$$

where we remark that surfaces of constant ξ do not (in general) coincide with surfaces of constant t (they can coincide only for a given initial fixed $t = t_i$ identified with an initial ξ_i).

In terms of ξ, and using (16) and (17), the system (13*a*–13*h*) becomes

$$\frac{\partial \Omega_b}{\partial \xi} = \Omega_b \left[-1 + \Omega_m + (1+3\,w)\,\Omega_e + \Omega_b\right], \tag{27a}$$

$$\frac{\partial \Omega_m}{\partial \xi} = \Omega_m \left[-1 + 3\,\alpha + \Omega_m + (1+3\,w)\,\Omega_e + \Omega_b\right] + 3\,\alpha\Omega_e, \tag{27b}$$

$$\frac{\partial \Omega_e}{\partial \xi} = \Omega_e \left[-1 - 3\,w - 3\,\alpha + \Omega_m + (1+3\,w)\,\Omega_e + \Omega_b\right] - 3\,\alpha\Omega_m, \tag{27c}$$

$$\begin{aligned}\frac{\partial \delta^{(\mathcal{H})}}{\partial \xi} =& -\delta^{(\mathcal{H})}\left(1+3\delta^{(\mathcal{H})}\right) + \frac{\Omega_m\,\left(\delta^{(\mathcal{H})}-\delta^{(m)}\right)}{2} \\ &+ \frac{(1+3w)\Omega_e\,\left(\delta^{(\mathcal{H})}-\delta^{(e)}\right)}{2} + \frac{\Omega_b\,\left(\delta^{(\mathcal{H})}-\delta^{(b)}\right)}{2},\end{aligned} \tag{27d}$$

$$\frac{\partial \delta^{(b)}}{\partial \xi} = -3\delta^{(\mathcal{H})}\left[1+\delta^{(b)}\right], \tag{27e}$$

$$\begin{aligned}\frac{\partial \delta^{(m)}}{\partial \xi} =& -3\left(1+\delta^{(m)}\right)\delta^{(\mathcal{H})} + 3\,\alpha\,\delta^{(m)} - \frac{3\,\alpha\,\delta^{(m)}\,(\Omega_m+\Omega_e)}{\Omega_m} \\ &+ \frac{3\,\alpha\,\delta^{(\mathcal{H})}\,(\Omega_m+\Omega_e)}{\Omega_m} + \frac{3\,\alpha\,\delta^{(e)}\,\Omega_e}{\Omega_m},\end{aligned} \tag{27f}$$

$$\begin{aligned}\frac{\partial \delta^{(e)}}{\partial \xi} =& -3\left(1+w+\delta^{(e)}\right)\delta^{(\mathcal{H})} - 3\,\alpha\,\delta^{(e)} + \frac{3\,\alpha\,\delta^{(e)}\,(\Omega_m+\Omega_e)}{\Omega_e} \\ &- \frac{3\,\alpha\,\delta^{(\mathcal{H})}\,(\Omega_m+\Omega_e)}{\Omega_e} - \frac{3\,\alpha\,\delta^{(m)}\,\Omega_m}{\Omega_e}.\end{aligned} \tag{27g}$$

The autonomous dynamical system (27*a*–27*g*) has seven-dimensions and can be numerically solved for initial conditions given at a fixed $\xi = \xi_i$ for each comoving shell $r = r_i$.

The density variables Ω_b, Ω_m and Ω_e form a separate subsystem (as eqs. (27*a*–27*c*) do not depend on the δ functions). Hence, this subsystem is an invariant subspace of (27*a*–27*g*), formally identical to the dynamical system that would be obtained for Ω functions of the corresponding FLRW model with null δ functions. We will refer to the set (27*a*–27*c*) as the homogeneous projection (subsystem). On the other hand, the δ functions depend on both δ and Ω functions, and only form an independent subsystem when the Ω are constant during the evolution (i.e., when Ω functions do not evolve at the critical points of the homogeneous projection). We will refer to the set of δ functions evolution equations (27*d*–27*g*) as the inhomogeneous projection. It is possible to fully represent the solution for a set of initial conditions at a given shell $r = r_i$ by means of a trajectory evolution 3-dimensional plot in the homogeneous phase-space plus the evolution of the δ functions vs. ξ (or vs. t).

The QL scalar $\mathcal{H}_q(\xi, r_i)$ is related to the Ω functions as‡

$$\frac{\partial \mathcal{H}_q}{\partial \xi} = \frac{\dot{\mathcal{H}}_q}{\mathcal{H}_q} = -\mathcal{H}_q\left(1 + \frac{1}{2}\Omega_b + \frac{1}{2}\Omega_m + \frac{1+3w}{2}\Omega_e\right). \tag{28}$$

‡ In fact, for the numerical work it is convenient to add equation (28) to the system (27*d*–27*g*), and solve the resulting 8–dimensions system for a given set of initial conditions related by the constraints.

Table 1. The critical points and their respective eigenvalues of the system (27*a*–27*c*).

Critical points	$(\Omega_b, \Omega_m, \Omega_e)$	Eigenvalues ($\Delta = \sqrt{1+4(\alpha/w)}$)
P1	$(0, \frac{(1+\Delta)}{2}, \frac{(1-\Delta)}{2})$	$\lambda_1 = -3w\Delta$, $\lambda_2 = \frac{3w}{2}(1-\Delta)$, $\lambda_3 = 1+\frac{3w}{2}(1-\Delta)$
P2	$(0, \frac{(1-\Delta)}{2}, \frac{(1+\Delta)}{2})$	$\lambda_1 = \frac{3w}{2}(1+\Delta)$, $\lambda_2 = 1+\frac{3w}{2}(1+\Delta)$, $\lambda_3 = 3\,w\Delta$
P3	(1, 0, 0)	$\lambda_1 = -\frac{3w}{2}(1-\Delta)$, $\lambda_2 = -\frac{3w}{2}(1+\Delta)$, $\lambda_3 = 1$
P4	(0, 0, 0)	$\lambda_1 = -1-\frac{3w}{2}(1-\Delta)$, $\lambda_2 = -1-\frac{3w}{2}(1+\Delta)$, $\lambda_3 = -1$

From the numerical solutions Ω_b, Ω_m, Ω_e, $\delta^{(b)}$, $\delta^{(m)}$, $\delta^{(e)}$, $\delta^{(\mathcal{H})}$ and $\mathcal{H}_q(\xi, r_i)$, it is possible to compute the rest of the scalars that characterize the LTB metric: the QL baryonic, CDM and DE densities from (22), the spatial curvature and its fluctuation $\delta^{(\kappa)}$ from the constraints (25), and the corresponding local scalars $A = \mathcal{H}$, $\mathcal{K}$, ρ_b, ρ_m, ρ_e, J from $A = A_q(1+\delta^A)$.

The cosmic physical time can be computed as well at a fixed $\xi(t,r)$ and $r = r_i$ [25]

$$t(r_i) = \int_0^{\xi(t,r_i)} \frac{d\xi'}{\mathcal{H}_q(\xi', r_i)}. \tag{29}$$

And finally, the scalars appearing in LTB metric can be computed as $R = \exp\left(\int \mathcal{H}_q dt\right)$ and $R' = R\exp\left(-\int \mathcal{H}_q \delta^{(\mathcal{H})} dt\right)$.

3.1. Homogeneous subspace

We obtain the critical points of (27*a*–27*c*) by solving the algebraic quadratic equations that follows by setting to zero their right–hand side. We also compute the eigen–value set related to each critical point by linearization of the homogeneous system near the critical points, by means of the jacobian matrix of the dynamical system. The findings are summarized in table 1.

Points $P1$, and $P2$ could be mathematically correct but non–physical (complex solutions or negative defined real numbers), for general values of α and w. As $w < -1/3$ for FLRW DE models (DE being the responsible of the late accelerated expansion stage of the universe), we see that the points are real for $\alpha \leqslant -w/4$. This result is discussed in [9] in the context of FLRW cosmology. Considering the FPs for the interaction that fulfills the observational bounds obtained in [7, 8, 9, 34], we see that both points are always physical when w is close to/lower than -1, and $\alpha < 0.25$.

Also, it is possible to obtain non–negative $P1$ and $P2$ when $\alpha > 0$. While [30] considers also the evolution of the metric (1) with $\alpha < 0$ (for a different coupling term), in the present article we will restrict ourselves to $\alpha > 0$ in order to study the relevance of the critical points $P1$ and $P2$ on the dynamics of the metric (1). The study of the phase space evolution will be undertaken by looking at the trajectories in terms of the corresponding homogeneous projection.

The critical points and their respective eigen–values are displayed in Table (1). Considering $w \sim -1$ and $0 < \alpha \leq -w/4$, it is possible to determine the behavior of the trajectories near the critical points. The critical point $P1$ is a saddle point as $\lambda_1 > 0$ while the rest of the eigenvalues are strictly negative. The critical point $P2$ is a future attractor (with negative eigenvalues). $P3$ is a past attractor with all eigenvalues strictly positive. Finally, $P4$ is a saddle point as $\lambda_1, > 0$ while $\lambda_2, \lambda_3 < 0$.

The points of the homogeneous subspace that live on the plane $M \equiv \Omega_b + \Omega_m + \Omega_e = 1$ (and from (24), $M \equiv \Omega_{\mathcal{K}} = 0$) form an invariant subspace. Defining a vectorial base of the homogeneous subsystem $\{\boldsymbol{u_1}, \boldsymbol{u_2}, \boldsymbol{u_3}\}$ as the orthonormal vectors in the direction of the Ω_b, Ω_m, and Ω_e axis, respectively, it is possible to define a new base $\{\boldsymbol{v_1}, \boldsymbol{v_1}, \boldsymbol{n}\}$, where $\boldsymbol{v_1}, \boldsymbol{v_1}$ are two linear independent vectors generating the invariant plane while $\boldsymbol{n} = (\boldsymbol{u_1} + \boldsymbol{u_2} + \boldsymbol{u_3})/\sqrt{3}$ is the normal vector to the plane. Any trajectory curve in the phase space is written as

$$\begin{aligned} \boldsymbol{\Omega}(\xi) &= \Omega_b(\xi)\boldsymbol{u_1} + \Omega_m(\xi)\boldsymbol{u_2} + \Omega_e(\xi)\boldsymbol{u_3} \\ &= \Omega_1(\xi)\boldsymbol{v_1} + \Omega_2(\xi)\boldsymbol{v_1} + \Omega_n(\xi)\boldsymbol{n} \end{aligned} \tag{30}$$

where $\Omega_i(\xi) = \boldsymbol{\Omega} \cdot \boldsymbol{v_i}$ with $i = 1, 2$ and $\Omega_n(\xi) = \boldsymbol{\Omega} \cdot \boldsymbol{n} = (\Omega_b + \Omega_m + \Omega_e)/\sqrt{3}$. We can solve the evolution of the trajectories in the direction of the second base from eqs. (27*a*-27*c*). In particular,

$$\begin{aligned} \frac{d}{d\xi}\Omega_n &= \frac{1}{\sqrt{3}}\left(\frac{d\Omega_b}{d\xi} + \frac{d\Omega_m}{d\xi} + \frac{d\Omega_e}{d\xi}\right) \\ &= \frac{1}{\sqrt{3}}\left((\Omega_b + \Omega_m + \Omega_e - 1)(\Omega_b + \Omega_m + \Omega_e + 3w\Omega_e)\right). \end{aligned} \tag{31}$$

From the relation of above it is clear that the trajectories with $\Omega_b + \Omega_m + \Omega_e - 1 = -\Omega_{\mathcal{K}} = 0$ at any point do not evolve in the direction of $\boldsymbol{n}$, and, consequently, live in the invariant plane entirely. , as for any point $P \in M$

$$\left[\frac{d}{d\xi}\left(\Omega_b + \Omega_m + \Omega_e\right)\right]_P = 0. \tag{32}$$

The trajectories in the homogeneous phase space cannot cross the invariant subspace M [30, 31], so they maintain the same $\Omega_{\mathcal{K}}$ sign during their entire evolution. The homogeneous subspace is divided in three separate regions: trajectories for which $\Omega_{\mathcal{K}} = 0$, trajectories with $\Omega_{\mathcal{K}} > 0$, and trajectories with $\Omega_{\mathcal{K}} < 0$.

Given that the critical points P1, P2, and P3 are on the invariant plane (P2 and P3 being future and past attractors, respectively), it seems contradictory for the trajectories with non null curvature to evolve to/from them. At this point, it is important to stress that the trajectory evolution to the point P2, independently of the curvature, is asymptotical, i.e., in the limit $L \to \infty$ in the expanding LTB solution. From (20), we know $\mathcal{K}_q$, ρ_{bq} evolve as L^{-2} and L^{-3}, respectively, while both ρ_{mq} and ρ_{eq} evolve as an addition of a term with L^{γ_1} plus a term with L^{γ_2}. When $L \to \infty$, $\mathcal{K}_q$, ρ_{bq} will become much smaller than ρ_{mq} and ρ_{eq} as $\gamma_1 > -2$ for the FPs considered. The same discussion applies to the past attractor $P3$ as $L \to 0$, the baryonic matter ρ_{bq} has asymptotical values greater than those of $\mathcal{K}_q$, ρ_{mq}, and ρ_{eq} in the past and is the dominant source ($-3 < \gamma_2$). On the other hand, considering an additional uncoupled radiation source, as in [31], we would find that the point P3 is no longer a past attractor but a saddle point and a new past attractor appears where only the radiation source is non null (with QL energy density scaling as L^{-4}). It is convenient to consider the radiation source in order to obtain the standard Cosmology radiation expansion stage.

3.2. Complete dynamical system critical points

Fixing the Ω functions to the values given by the homogeneous critical points, we now find the inhomogeneous part of them by solving the δ functions values that make the

right hand side of eqs. (27*d*-27*g*) null. We also study the behaviour of the system in the vicinity of the points by finding the eigen-values of the jacobian matrix of the complete system at the points. Some mathematical solutions for the critical points include δ functions lower than -1 for some choices of parameters, we will consider that these solutions are not compatible with the spherical symmetry. As discussed in [30, 31], a δ function evolving to values lower than -1 could be interpreted as a break in the spherical symmetry that should be addressed with a more general metric, such as the non–spherical Szekeres metric. For the critical points of the homogeneous subspace P3 and P4, Ω_m and Ω_e are null and the right hand side of eqs. (27*f*,27*g*) cannot be evaluated as some terms depend on the ratio Ω_m/Ω_e, or its inverse. However, in the vicinity of the points P3 and P4, we will study the corresponding eigen-values of the jacobian matrix of the complete system in the limit

$$lim_{(\Omega_m,\Omega_e)\to(0,0)}\frac{\Omega_e}{\Omega_m}=k. \tag{33}$$

The limit of above depends strongly on the curve $\Omega_e=\Omega_e(\Omega_m)$ considered in the plane $\Omega_e-\Omega_m$. If we assume a curve such that the limit is a non-null constant k, it is possible to find the eigen–values of the critical points as a function of the FPs and also the direction constant k.

As mentioned in the above subsection, in the case of the point P3, the limit $(\Omega_m,\Omega_e)\to(0,0)$ must be interpreted asymptotically (i.e., when $L\to 0$). Given the scaling laws ruling the evolution of ρ_{mq} and ρ_{eq} for this coupling with the terms proportional to L^{γ_2} being dominant over the terms with L^{γ_1} as $\gamma_1>\gamma_2$,

$$lim_{L\to 0}\frac{\Omega_e}{\Omega_m}=\frac{(\rho_{eq0}(1-a)+\rho_{mq0}b)L^{\gamma_2}}{(\rho_{mq0}a-\rho_{eq0}b)L^{\gamma_2}}=\frac{1-\Delta}{1+\Delta} \tag{34}$$

and, consequently, the direction of the limit near P3 is $k=(1-\Delta)/(1+\Delta)<1$, independently of the shell $r=r_i$ considered.

- P1: When the homogeneous part takes the form of the critical point P1, we find four different critical points:
  - Saddle Point P1a: $\delta^{(\mathcal{H})}=0,\delta^{(b)}$arbitrary$,\delta^{(m)}=0,\delta^{(e)}=0$. While four of the corresponding eigen–values are identical to these of the P1 that are listed in table 3.1 (with two of them equal to λ_3, we find a null eigen–value (with eigen–vector in the direction of the $\delta^{(b)}$ axis) and, finally, the eigen–value $\lambda=(-3/2)(1+w(1-\Delta)/2)$. This point is a saddle point for the ranges of FPs considered.
  - Points P1b,P1c,P1d: where $\delta^{(\mathcal{H})}$ is one of the roots of the polynomial

$$12\,{\delta^{(\mathcal{H})}}^3+a_1{\delta^{(\mathcal{H})}}^2+a_2\delta^{(\mathcal{H})}+a_3=0, \tag{35}$$

$$a_1=3\,w\Delta-24\,\alpha-15\,w+2 \tag{36}$$

$$a_2=-6\Delta\alpha\,w+4\,w\Delta+12\,\alpha\,w-6\,w-2 \tag{37}$$

$$a_3=(1-\Delta)(3w^3+4w^2+6\alpha w)+6\alpha w^2+4\alpha+2w \tag{38}$$

    and $\delta^{(b)}=-1$, $\delta^{(m)}=-1+2\alpha(\delta^{(\mathcal{H})}-w)/((\Delta+1)(\delta^{(\mathcal{H})}-2\alpha-w))$, $\delta^{(e)}=-1-(w^2(\Delta-1)+w(\Delta+3)\delta^{(\mathcal{H})})/(2(\delta^{(\mathcal{H})}-2\alpha-w))$. The eigen–values should be determined in a case by case basis. For example, when $w=-1$ and $\alpha=0.1$, only two of the critical points are physical and both are saddle points.

- P2: Assuming the homogeneous critical point P2, we find different choices of the δ functions that make the right hand side of eq. (27*d*–27*g*) null. One of them is a future attractor:
  - Future attractor P2a: $\delta^{(\mathcal{H})}=0, \delta^{(b)}$arbitrary, $\delta^{(m)}=0, \delta^{(e)}=0$. In this case, the corresponding eigen–values are negative defined for any choice of the FPs: four identical to these of the P2 that are listed in table 3.1, a null eigen–value (with eigen–vector in the direction of the $\delta^{(b)}$ axis) and, finally, the eigen–value $\lambda=(-3/2)(1+w(1+\Delta)/2)$, which is negative for the choices of w and α considered. We conclude that this point act as a future attractor. As this point represents a future asymptotic point (when $L\to\infty$) for which the baryonic matter has a much lower contribution than the dark sources, the value of $\delta^{(b)}$ is irrelevant. For the dark sources, both δ functions tend to null, which correspond to a homogeneous metric.
  - Points P2b, P2c,P2d: where $\delta^{(\mathcal{H})}$ is one of the solutions to
$$12\,{\delta^{(\mathcal{H})}}^3+b_1{\delta^{(\mathcal{H})}}^2+b_2\delta^{(\mathcal{H})}+b_3=0, \tag{39}$$
$$b_1=-3\,w\Delta-24\,\alpha-15\,w+2 \tag{40}$$
$$b_2=6\Delta\alpha\,w-4\,\Delta w+12\,\alpha\,w-6\,w-2 \tag{41}$$
$$b_3=(1+\Delta)(3w^3+4w^2+6\alpha w)+6\alpha w^2+4\alpha+2w \tag{42}$$
    and $\delta^{(b)}=-1$, $\delta^{(m)}=-1+2\alpha(\delta^{(\mathcal{H})}-w)/((1-\Delta)(\delta^{(\mathcal{H})}-2\alpha-w))$, $\delta^{(e)}=-1-(w^2(\Delta-1)+w(\Delta+3)\delta^{(\mathcal{H})})/(2(\delta^{(\mathcal{H})}-2\alpha-w))$. This points should be treated similarly to the points P1b-P1c, in a case by case basis, e.g., when $w=-1$ and $\alpha=0.1$, only two of them are physical and they both behave as saddle points.
- P3: In this case, $k=(1-\Delta)/(1+\Delta)$ and we find three critical points of the complete system: two saddle points and an past attractor:
  - Saddle point P3a: $\delta^{(\mathcal{H})}=0, \delta^{(b)}=0, \delta^{(m)}$arbitrary, $\delta^{(e)}=\delta^{(m)}$. In this case, the diverging terms on eq. (27*f*,27*g*) cancel and the corresponding eigen–values can be computed independently on the value of k. Four eigen–values take the same form as these in table 3.1 for P3 (with two of them identical to λ_3), one eigen–value is null, and the remaining are $-3/2$,and $3\alpha\frac{1-k^2}{k}>0$, respectively. This point behave as a saddle point.
  - Past attractor P3b: $\delta^{(\mathcal{H})}=-1/2, \delta^{(b)}=-1$, $\delta^{(e)}=\delta^{(m)}$ and
$$\delta^{(m)}=-1-\frac{2\alpha^2(k^2+1)+2\alpha k^2(w+1)+4\alpha^2k+\alpha\,k}{2\alpha k^2-2\alpha-k}, \tag{43}$$
    In this case, we find two eigen–values that are defined as $3/2$, another one is $5/2$, three are defined as λ_1, λ_2 and λ_3 from P3 in table 3.1, and finally, the last eigen–value is $-3w\Delta+3/2>0$. As all of them are positive defined, we conclude that P3b is a past attractor.
  - Saddle Point P3c: $\delta^{(\mathcal{H})}=1/3, \delta^{(b)}=-1$, $\delta^{(e)}=\delta^{(m)}$ and
$$\delta^{(m)}=-1-\frac{3\alpha^2(k^2+1)+3\alpha k^2(w-1)+6\alpha^2k-\alpha k}{3\alpha k^2-3\alpha-k}, \tag{44}$$
    Two eigen–values are equal to -1 independently on the FPs, while the rest of them depend on w and α. For the range of parameters considered, we find at least two of the latter positive. Consequently, this is a saddle point.
- P4 Finally, for $P4$, we find two different critical points that are saddle points:

- Saddle point P4a: $\delta^{(\mathcal{H})}=0, \delta^{(b)}$arbitrary, $\delta^{(m)}$arbitrary, $\delta^{(e)}=\delta^{(m)}$. One eigen–value take the form of λ_1 for P4 in table 3.1, one is λ_2, while two of them are $\lambda_3=-1$, two are null and the remaining eigen–value depends on the direction k. This point behave as a saddle point.
- Saddle Point P4b: $\delta^{(\mathcal{H})}=-1/3, \delta^{(b)}=-1$, and

$$\delta^{(m)} = -1-\frac{3\alpha^2(k^2+1)+3\alpha k^2(w+1)+6\alpha^2 k+\alpha k}{3\alpha k^2-3\alpha-k}, \quad (45)$$

$$\delta^{(e)} = -1-\frac{3\alpha^2(k^2+1)+3\alpha k^2 w+6\alpha^2 k-\alpha(k+1)+kw}{3\alpha k^2-3\alpha-k} \quad (46)$$

  In this case, two eigen–values correspond to λ_1 and λ_2 for P4 in table 3.1, respectively, two eigen–values are $\lambda_3=-1$, while we find two eigen–values with values $+1$, and two that depend on the choice of the FPs and the constant k. We conclude that this is a saddle point.

The past attractor point P3b and the future attractor P2a are of particular interest. In the next section, we define an initial profile example for which some computed trajectories evolve asymptotically from P3b to P2a.

4. Initial profile leading to a structure formation example.

For some choices of initial profiles, we find a special kind of evolution for which some shells in the vicinity of the symmetry center (inner shells) $\mathcal{H}_q=0$ at a finite time $t=t_{\max}(r_i)$, the maximum expansion instant, while, for the rest of the shells (outer shells), $\mathcal{H}_q$ evolve smoothly [30, 31]. For the inner shells, the QL curvature $\mathcal{K}_q$ is necessarily positive ($\Omega_{\mathcal{K}}<0$) and the turning point is defined as

$$\mathcal{K}_q(r_i)=\frac{\kappa}{3}\left[\rho_{bq}+\rho_{mq}+\rho_{eq}\right]_{r_i,t_{\max}}. \quad (47)$$

At the maximum expansion instant, the corresponding Ω scalars of the inner shells diverge while their corresponding QL energy–densities are finite. The evolution of the inner shells right after the maximum expansion instant cannot be described with the same LTB metric, but it is possible to match a contracting LTB solution for the inner shells with QL scalars defined by continuity, and, thus, obtain a spherically symmetric structure formation toy model. In terms of the dynamical system eqs. (27*a*-27*g*), a solution with divergent Ω_b, Ω_m, and Ω_e is not enough to define the spherical collapse toy model as some shell–crossing singularities can be present.

In this section, proceeding as in [30, 31], we set the necessary conditions to avoid well-known singularities of the LTB metric, and we next define a set of local densities profiles and spatial curvature in order to numerically solve the evolution in ξ at a fixed shell $r=r_i$. For the radial coordinate r, we consider $r\in[0,r_{\max}]$ while r_i is the element of an n-partition (defined as $r_i=ir_{\max}/n$). The initial conditions are defined at the hypersurface $t=t_0$ (subindex 0 is used for the different scalar evaluated at the instant t_0).

4.1. Shell–cross singularities.

The QL scalar formalism cannot be used at shell crossing singularities (as the delta functions are divergent). Thus, the initial conditions considered in the numerical work must avoid an evolution towards a shell crossing, i.e., $\Gamma>0$ must hold throughout the evolution. For LTB dust solutions with $\Lambda=0$ it is possible to state analytic

restrictions on initial conditions to guarantee an evolution with no shell crossings ([15, 16, 17, 20]), but for the solutions with nonzero pressure that we are considering here this can only be achieved by numerical trial and error of initial conditions.

In order to integrate the system $(27a)$–$(27g)$, we can compute the initial conditions from a given set of initial profiles $\rho_{b0}(r), \rho_{e0}(r), \rho_{m0}(r)$ and $\mathcal{K}_0(r)$ and a defined $R_0(r)$. The QL scalars initial profiles $\rho_{bq0}(r)$, $\rho_{eq0}(r)$, ρ_{mq0}, $\mathcal{K}_{q0}(r)$ and the fluctuations $\delta_0^{(m)}$, $\delta_0^{(e)}$, $\delta_0^{(\mathcal{H})}$ follow directly from (7) with $R = R_0$. For simplicity, it is convenient to consider $\xi_0 = \xi(t_0, r) = 0$ for all r§, which leads to: $\Omega_{b0} = \Omega_b(0, r)$, $\Omega_{e0} = \Omega_e(0, r)$, $\Omega_{m0} = \Omega_m(0, r)$, $\delta_0^{(b)} = \delta^{(b)}(0, r)$, $\delta_0^{(m)} = \delta^{(m)}(0, r)$, $\delta_0^{(e)} = \delta^{(e)}(0, r)$ and $\delta_0^{(\mathcal{H})} = \delta^{(\mathcal{H})}(0, r)$.

The initial profiles could evolve to a shell crossing singularity, so we carefully test the evolution of Γ to verify that $\Gamma > 0$ holds for all ξ. It is convenient to relate Γ to $\delta^{(\kappa)}$ by deriving with respect to radial coordinate the scaling laws (20)

$$\delta^{(\kappa)} = -\frac{2}{3} + \frac{\frac{2}{3} + \delta_0^{(\kappa)}}{\Gamma} \quad \Rightarrow \quad \Gamma = \frac{\frac{2}{3} + \delta_0^{(\kappa)}}{\frac{2}{3} + \delta^{(\kappa)}}, \tag{48}$$

which we can rewrite, from (25), as

$$\Gamma = \frac{\Omega_{\mathcal{K}}(t, r)}{\Omega_{\mathcal{K}}(0, r)} \left(\frac{\Omega_{b0}(\delta_0^{(b)} + \frac{2}{3}) + \Omega_{m0}(\delta_0^{(m)} + \frac{2}{3}) + \Omega_{e0}(\delta_0^{(e)} + \frac{2}{3}) - 2\delta_0^{(\mathcal{H})} - \frac{2}{3}}{\Omega_b(\delta^{(b)} + \frac{2}{3}) + \Omega_m(\delta^{(m)} + \frac{2}{3}) + \Omega_e(\delta^{(e)} + \frac{2}{3}) - 2\delta^{(\mathcal{H})} - \frac{2}{3}} \right). \tag{49}$$

From the expression of above, it is clear that Γ tends to null as $\delta^{(b)}$, $\delta^{(m)}$, $\delta^{(e)}$ diverge. On the other hand, Γ do not mandatorily diverge as $\mathcal{H}_q$ tends to zero. In the later case, the Ω functions and $\delta^{(\mathcal{H})}$ in the denominator will diverge, but the factor $\Omega_{\mathcal{K}}(t, r)$ will diverge as well at the same rate as the rest of the Ω functions and faster than $\delta^{(\mathcal{H})}$ ($\delta^{(\mathcal{H})}$ and the Ω functions inversely proportional to $\mathcal{H}_q$ and to $\mathcal{H}_q^2$, respectively). In general, an evolution of the models that is free from shell crossings needs to be determined numerically from (49).

4.2. Initial profiles, evolution and collapse time

As mentioned in [30], the LTB metric has a scale invariance that allows us to define dimensionless quantities: cosmic time $\bar{t} = H_0 t$, Hubble factor $\bar{\mathcal{H}}_q = \mathcal{H}_q / H_0$, and local densities $\kappa\bar{\rho}_a/3 = \kappa\rho_a/(3H_0^2)$ with H_0 an arbitrary constant (typically chosen as the present day Hubble factor in units $Km/(Mpc \cdot s)$ in cosmology) and subindex $a = b, m, e$. For the numerical work in this section, we take the time units with $H_0 = 1$ and energy density units with $\kappa/(3H_0^2) = 1$.

We consider the initial local profiles

$$\begin{aligned}
\rho_{b0} &= b_{10} + \frac{b_{11} - b_{10}}{1 + \tan^2(r)}, \qquad b_{10} = 0.90, \quad b_{11} = 1.20; \\
\rho_{m0} &= m_{10} + \frac{m_{11} - m_{10}}{1 + \tan^2(r)}, \qquad m_{10} = 1.00, \quad m_{11} = 13.10; \\
\rho_{e0} &= e_{10} + \frac{e_{11} - e_{10}}{1 + \tan^2(r)}, \qquad e_{10} = 0.90, \quad e_{11} = 1.66; \\
\mathcal{K}_0 &= k_{10} + \frac{k_{11} - k_{10}}{1 + \tan^2(r)}, \qquad k_{10} = -1.10, \quad k_{11} = 2.50;
\end{aligned} \tag{50}$$

§ It is possible to set $\xi = 0$ to define the same hypersurface as $t = t_0$, and from this point on, t and ξ hypersuperfaces will differ.

and $R_0(r) = \tan(r)$, with an r coordinate partition has $n = 20$ elements from 0 to $r_{\max} = \pi/2$. This choice is specially useful for the numerical work, as it would be possible to define a physical $\mathfrak{R}$ coordinate from R_0 and r as $\mathfrak{R} = \tan(r)$ for which $\mathfrak{R} = 0$ correspond to $r = 0$ (the symmetry center) and $\mathfrak{R} \to \infty$ as $r \to r_{\max}$. For the FPs, we chose $w = -1$, as in this case DE represents a well known cosmological constant. Although the observational bounds in [7, 8, 9, 34] on the parameter α for this interaction suggest a value close to zero (of order ~ 0.001), we take $\alpha = 0.1$ in order to stress the effect of the coupling term on the dynamics.

The initial profiles of above evolve to a LTB collapse scenario as some shells with values of $r = r_j$ around the symmetry centre $r = 0$ initially expand ($\mathcal{H}_q(t, r_j) > 0$), then bounce as $\mathcal{H}_q(t = t_{\max}, r_j) = 0$ and, finally, collapse ($\mathcal{H}_q$ negative), whereas the rest shells expand. For each bouncing shell with $r = r_j$, it is possible to numerically compute $t = t_{\max}$. As the inner shells evolve to the bounce instant, Ω_b, Ω_e, $\Omega_m \to \infty$. In this numerical example, we do not address the collapsing stage of evolution of the inner shells.

Figure 1 depicts the evolution of Ω_b, Ω_m and Ω_e for the different shells of the partition of r plotted in the phase–space of the homogeneous subsystem. We have plotted $\arctan(\Omega)$ in order to obtain a finite value of this function when $\Omega \to \infty$ (as $\Omega \to \infty$ implies $\arctan(\Omega) \to \pi/2$). Red dots represent the initial conditions for every shell $r = r_i$ in the radial partition. From the numerical results we notice that the first and second shells $j = 1, 2$ (close to the symmetry center) evolve from the past attractor $P3$ to infinity (corresponding to the instant when $\mathcal{H}_q = 0$ if no shell crossing singularities occur), while the rest of shells evolve from the past attractor $P3$ to the future attractor $P2$. Also, the trajectories evolve near the vicinity of the saddle point $P1$, stressing its behavior as an attractor in the direction of the eigenvector parallel to Ω_b (related to the corresponding eigenvalue λ_2 in 3.1). This attractor is unstable in the plane generated by the eigenvectors related to λ_1, λ_2 in 3.1. The later unstable plane is parallel to the plane $\Omega_b = 0$. This numerical example representation in the homogeneous projection allows us to have a better understanding of the critical points of the homogeneous projection.

In order to check for possible shell crossing singularities for this profile, it is necessary to compute evolution of $\delta^{(m)}$, $\delta^{(e)}$, $\delta^{(b)}$ and $\delta^{(\mathcal{H})}$ for all the shells. As discussed above, if $\delta^{(m)}$, $\delta^{(e)}$, $\delta^{(b)}$ tend to infinity if $\Gamma \to 0$ that marks a shell crossing singularity. As shown in figure 2, the values of $\delta^{(m)}$, $\delta^{(e)}$, $\delta^{(b)}$ for all ξ remain bounded and thus no shell crossing singularities occur for the initial profile. The function $\delta^{(\mathcal{H})}$ diverges as $\mathcal{H}_q$ tend to null for the inner shells, as expected from its definition $\delta^{(\mathcal{H})} = \mathcal{H}/\mathcal{H}_q - 1$, but, as discussed previously, Γ do not tend to null for those shields as the factor $\Omega_{\mathcal{K}}$ in (49) is inversely proportional to $\mathcal{H}_q^2$ and, consequently, $\delta^{(\mathcal{H})}/\Omega_{\mathcal{K}} \to 0$ as $\mathcal{H}_q \to 0$.

In figure 2, we see how the δ functions of the outer shells evolve towards the critical point P2a. For the larger ξ values, $\delta^{(\mathcal{H})}$, $\delta^{(m)}$ and $\delta^{(e)}$ tend to null for all the shells, and $\delta^{(b)}$ tend to an arbitrary value. In this numerical example and in the limit $L \to 0$, the ratio Ω_m/Ω_e tends to the constant $k = 0.1270$, which leads to the positive defined eigen–values of P3b, i.e., in this example, P3b acts as a past attractor for all the shells. Consequently, we find that the δ functions evolve in the past to the values found in the point P3b: $\delta^{(\mathcal{H})}$ tends to $-1/2$ in the past, $\delta^{(b)}$ tends to -1, while $\delta^{(m)}$ and $\delta^{(e)}$ tend to the corresponding values of eqs. (43, 43), which is -0.8873 for both functions.

With the numerical solution of the dynamical system, we can compute $\mathcal{H}_q$ from

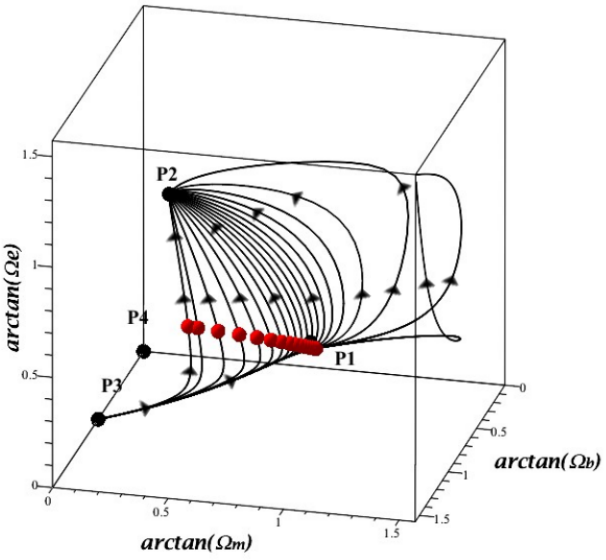

Figure 1. Phase-space trajectories of the homogeneous subsystem (27*a*–27*c*) with initial conditions (51) and FP $w = -1.0$, $\alpha = 0.1$. The red dots represent the initial values of Ω_b, Ω_m and Ω_e at every shell $r = r_i$ of the partition considered. The black points represent the critical points of the homogeneous projection from table 3.1.

(28), with the cosmic time t defined in (29). We can, then, plot implicitly the evolution of $\log(\mathcal{H}_q)$ vs. t for every shell $r = r_i$ of the partition. For the bouncing inner shells (r_1 and r_2 in this case), it is possible to evaluate numerically the cosmic time for which $\mathcal{H}_q = 0$ (asymptotic behaviour in $\log(\mathcal{H}_q)$): $t_{\max}(r_1) = 13.71$ and $t_{\max}(r_2) = 17.65$, respectively. Note that those cosmic times correspond to the maximum expansion of both shells. In figure 3, the curves $\log(\mathcal{H}_q)$ vs. t correspond to the shells r_1, r_2, r_3, and r_4.

The instant $t_{\max}(r_j)$ ($j = 1, 2$ for the numerical example of above) in our LTB model plays a role analogous to the turnaround time in the Newtonian spherical collapse model [35] or the collapse of a spherical perturbation in a FLRW background (see [36] and [37] for a top hat profile spherical collapse in an Einstein–de Sitter and a ΛCDM background, respectively), which in our scenario corresponds to the shells $r = r_j$ reaching their maximal expansion at different times $t = t_{\max}(r_i)$. Therefore, the numerical example we are presenting represents a collection of "bowler hat" profiles (smoothed "top hats") in which two shells of the partition collapse (with different values for $t_{\max}(r_i)$). It is reasonable then to average the values $t_{\max}(r_i)$ to obtain a single turnaround instant given by: $\langle t_{\max} \rangle = 15.68$.

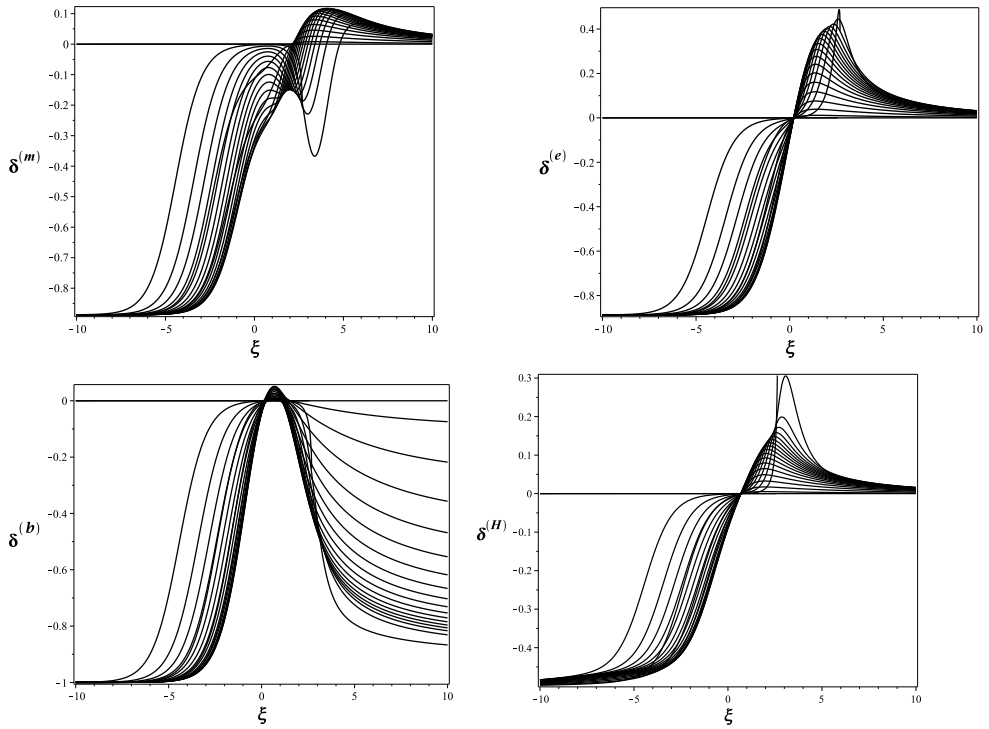

Figure 2. Evolution of $\delta^{(m)}$, $\delta^{(e)}$, $\delta^{(b)}$ and $\delta^{(\mathcal{H})}$ vs. ξ for shells $r = r_i$ with initial conditions given by (51) and $w = -1.0$, $\alpha = 0.1$. For all the shells, the δ functions evolve from the saddle point P3b in the past (negative values of ξ). For the outer shells, the δ functions evolve to the future attractor P2a.

Note that the average $\langle t_{\max} \rangle$ is obtained numerically, hence it depends, not only on the background dynamics: FPs w and α, energy densities/expansion rate of the background (as is the case in the collapse of spherical perturbations in a FLRW background), but also on the chosen local initial profiles. While a single turn around value $\langle t_{\max} \rangle$ can always be found, it is necessary to do it in a case by case basis on the full non-linear dynamics (as opposed to a linear order approximation in the spherical collapse model).

5. Interaction proportional to CDM and DE energy densities vs. other similar coupling terms

It is important to compare the results of the present article with those of previous work on the dynamics of LTB models described by evolution equations for the QL scalars for a different mixtures of coupled CDM and DE sources. In [31], the mixture that was considered consisted in two dark fluids coupled by an interaction term $J_q = 3\alpha\mathcal{H}_q\rho_{mq}$, which lead to a 5–dimensional autonomous dynamical system with the homogeneous projection defined by the functions Ω_m and Ω_e and the inhomogeneous projection defined by $\delta^{(m)}$, $\delta^{(e)}$ and $\delta^{(\mathcal{H})}$. In [30], we considered the same sources and a coupling term given by $J_q = 3\alpha\mathcal{H}_q\rho_{eq}$, with the addition of a radiation fluid in the homogeneous projection (dominant near the initial singularity) examined in an appendix.

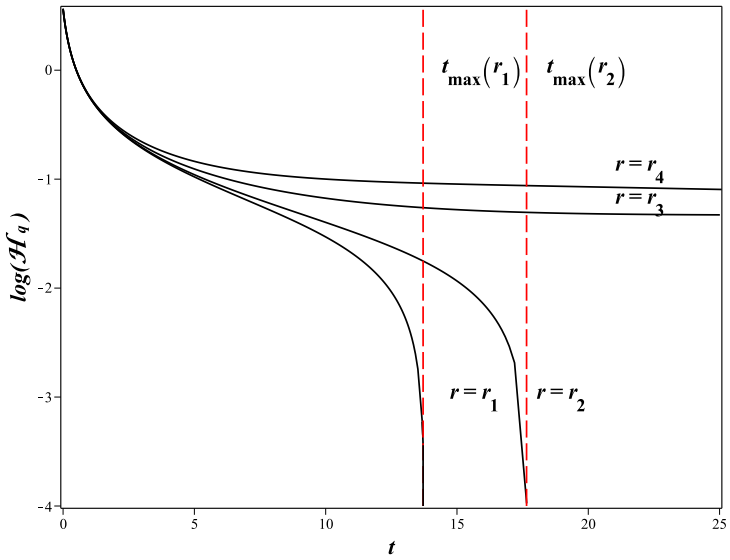

Figure 3. Evolution of $\log(\mathcal{H}_q)$ (from 28) vs. cosmic time t (defined in (29)) for shells r_1, r_2, r_3, and r_4 with initial conditions given by (51) and $w = -1.0$, $\alpha = 0.1$. While $\mathcal{H}_q$ of the inner shells r_1, r_2 tend to null, $\log(\mathcal{H}_q)$ tends asymptotically to $-\infty$. For outer shells r_3, r_4, $\mathcal{H}_q$ is a continuous function, so is $\log(\mathcal{H}_q)$.

In this work, we consider an additional non relativistic matter term (baryonic matter) which is consistent with the cosmological observations and the coupling term is more general: $J_q = 3\alpha\mathcal{H}_q(\rho_{mq} + \rho_{eq})$. As a consequence, the corresponding homogeneous projection is now 3–dimensional (Ω_b, Ω_m and Ω_e) and the inhomogeneous projection has an additional function $\delta^{(b)}$. The addition of the baryonic matter source makes the dynamical system study more complex, specially the inhomogeneous projection.

We can compare the homogeneous projection in this work with those of previous papers, as some similarities arise. On one hand, we see that the homogeneous projections in the three articles contain a similar future attractor, whose position is determined by the type of interaction considered, as well as by the FPs w and α (the future attractor has coordinates: $\Omega_m = 0, \Omega_e = 1$ in [31]; $\Omega_m = -\alpha/w, \Omega_e = 1 + \alpha/w$ in [30]; and $\Omega_b = 0, \Omega_m = (1-\Delta)/2, \Omega_e = (1+\Delta)/2$ with $\Delta^2 = 1 + 4\alpha/w$ in this work). On the other hand, the past attractor in both [31] and [30] (with coordinates $\Omega_m = 1 + \alpha/w, \Omega_e = -\alpha/w$ and $\Omega_m = 1, \Omega_e = 0$ respectively) can be easily related to the critical point $P2$ in the present work ($\Omega_b = 0, \Omega_m = (1+\Delta)/2, \Omega_e = (1-\Delta)/2$). Note that, while $P2$ is a saddle point, it behaves as a past attractor in the subspace $\Omega_m - \Omega_e$ (generated by the eigenvectors with positive defined eigenvalues), while it acts as an attractor in the direction parallel to Ω_b axis. We can conclude that the past attractor (whose position is dependent of the interaction and FP considered) of the previous papers changed to a saddle point when we add an extra baryonic matter source. In fact a new past attractor $P3$ is added in this work, which can play an interesting role in the evolution of the initial profiles.

An invariant line of the homogeneous projection was found in [30], connecting

the origin of the $\Omega_m - \Omega_e$ plane with the future attractor. In [31], we found also an invariant line connecting $\Omega_m = 0, \Omega_e = 0$ point and the past attractor. Given that no phase space trajectory can cross this later invariant line, some initial conditions, near the past attractor (and under this line) would end their evolution towards the $\Omega_e = 0$ axis (see figure 1 in [31]). Looking at the projection $\Omega_b = 0$ in the present paper, we see that neither the line that connects the origin with the saddle point $P2$ nor the line that connects the origin with the future attractor are invariant subspaces. Although there can still be trajectories that evolve to $\Omega_e = 0$ axis in this work, they are related to the $\Omega_b = 0$ projection and can be avoided in a cosmological scenario by considering an extra baryonic matter source.

For the interaction $J_q = 3\alpha\mathcal{H}_q(\rho_{mq} + \rho_{eq})$ in the 3-dimensional homogeneous projection, we find the invariant plane $\Omega_\mathcal{K} = -\mathcal{K}_q/\mathcal{H}_q^2 = 0$. In fact $\Omega_\mathcal{K} = 0$ is also an invariant subspace in the previous works, defined as the lines that connect the past and future attractors. In all the cases, the trajectories of the homogeneous phase–space can be classified according to their curvature sign: flat trajectories $\Omega_\mathcal{K} = 0$, where the shells evolve from the past attractor to the future attractor through the invariant line/plane; trajectories with $\Omega_\mathcal{K} < 0$, that evolve asymptotically from the past attractor to the future attractor according to their corresponding scaling laws maintaining the same sign in the curvature; and trajectories $\Omega_\mathcal{K} > 0$ that evolve asymptotically from the past attractor to the future attractor or to infinity (the later trajectories representing a collapse shell in the complete system description if no singularities are found).

In order to define the Γ function in [31] and [30], analytical solutions where studied for ρ_{mq} and ρ_{eq} in terms of the scale factor L. In [31] and because of the choice of the interaction, the function ρ_{mq} was particularly simple as $\rho_{mq} = \rho_{mq0}L^{-3(1-\alpha)}$, allowing us to connect the Γ function directly to $\delta^{(m)}$. On the other hand, in [30], it was ρ_{eq} that had a power law dependency on L as $\rho_{eq} = \rho_{eq0}L^{-3(1+w+\alpha)}$, which resulted in Γ being related to $\delta^{(e)}$. In the present paper with a more general interaction and the addition of the baryonic matter source, we find an analytical solution for ρ_{mq} and ρ_{eq} in terms of L but no simple power law was obtained for either one of them, making the Γ function dependent on $\delta^{(b)}$, $\delta^{(m)}$ and $\delta^{(e)}$.

Finally, it is worth considering the addition of a nearly homogeneous radiation-like source to the dynamical system, proceeding in a similar way as we did in the appendix in [30]. Such radiation source would yield a new function Ω_r that would be added to the set of phase space variables (with $\delta_r = 0$, since it would be homogeneous radiation), thus leading to a 4-dimensional homogeneous projection. It is natural to assume that the critical point $P3$ (related to a model without CDM or DE sources) would no longer be an attractor of the system, as a new attractor would appear at the value $\Omega_r = 1$, with the rest of the Ω functions vanishing. This attractor is easily understood given the evolution with the scale factor L of the QL scalars. The QL scalars ρ_{bq}, ρ_{mq} and ρ_{eq} would still evolve with L as in eq. (20), while $\rho_{rq} = \rho_{rq0}L^{-4}$. As $L \to 0$ for every shell, the radiation source would dominate the early expansion near the initial singularity in the same way as in [30].

As a concluding remark, the addition of the baryonic source and the consideration of a more general coupling term in this work added more complexity to the dynamical system analysis, but it is still possible to analyticaly obtain interesting information and a similar kind of numerical solutions as in previous articles.

6. Conclusions

We have generalized in the present paper the results of previous work [30, 31] by studying the dynamics of LTB solutions containing three sources: baryonic matter with interactively coupled CDM and DE. The coupling term we considered is a reasonable generalization of those used in the previous papers, as it is proportional to the addition of both dark sources energy densities (not only to one of them). Using the QL scalars formalism, we transformed the Einstein's evolution equations into a 7–dimensional autonomous dynamical system. The dynamical system can be decomposed in two subsystems: the 3–dimensional invariant homogeneous subsystem whose variables are the dimensionless QL scalars (Ω_b, Ω_m, Ω_e), related to the FLRW model, and a 4–dimensional subspace for the δ functions ($\delta^{(b)}, \delta^{(m)}$, $\delta^{(e)}$, $\delta^{(\mathcal{H})}$) that can be interpreted as exact deviations from the FLRW background.

For the homogeneous projection we obtained four critical points summarized in table 3.1: a saddle point $P1$, a future attractor $P2$, a past attractor $P3$ and a saddle point $P4$. The behavior of the critical points was examined under the assumption that w is of order/ lower than -1 and $0 < \alpha < 0.25$, based on the observational bounds that have been obtained for this coupling in FLRW cosmology [7, 8, 9, 34]. In the complete description and given the complexity of the dynamical system, up to thirteen critical points are found (some of them not compatible with spherical symmetry for some choices of the FPs, with $\delta < -1$). Of particular interest are the past attractor $P3b$ and the future attractor $P2a$, that should be considered as asymptotical points in the limits $L \to 0$ and $L \to \infty$ for the expanding LTB metric (L being a FLRW scale factor–like function), respectively. The future attractor shows a homogeneous LTB space where CDM and DE are dominant sources with null δ functions while curvature and baryonic matter have much smaller contributions. The δ functions are computed with a set of initial conditions in order to avoid shell crossing singularities (instant for which $\Gamma \to 0$, with Γ defined by (49)). To have $\Gamma > 0$ is a necessary condition to avoid shell crossing singularities for which $\delta^{(b)}, \delta^{(m)}$, $\delta^{(e)}$, $\delta^{(\mathcal{H})}$ diverge at finite evolution times.

Finally, in order to illustrate how to solve numerically the evolution equations we considered a specific example of a given set of initial profiles (51), with shell partition for the coordinate r and FPs ($w = -1$ and $\alpha = 0.1$). In this example, two inner shells (r_1 and r_2) evolved with Ω_b, Ω_m, Ω_e tending to infinity at a finite time while the outer shells evolve towards the future attractor (figure 1). As no shell crossing is present during the evolution (figure 2), we can conclude that the Ω_b, Ω_m, Ω_e diverging for the inner shells corresponds to a maximal expansion or "turn around" instant for which $\mathcal{H}_q = 0$ marks the outset of a collapse scenario. Because the LTB models are inhomogeneous these "turn around" instants occur at different cosmic times for different comoving observers, though it is possible to characterize these times as a single "turn around" by computing numerically (in a case by case basis) the average $\langle t_{\max} \rangle$ (figure 3). In this way we can relate this numerical computation to the single "turn around" time in "top hat" of spherical perturbations models discussed in the literature.

References

[1] Planck Collaboration I 2014 *Astron. Astrophys.* **571** 1
[2] Caldera-Cabral G., Maartens R. and Ureña-López L. A. 2009 *Phys. Rev. D* **79** 063518

[3] H. Ziaeepour, arXiv:astro-ph/0002400; M. Sami and T. Padmanabhan, Phys. Rev. D **67**, 083509 (2003); D. Comelli, M. Pietroni and A. Riotto, Phys. Lett. B **571**, 115 (2003); L. P. Chimento, A. S. Jakubi, D. Pavon and W. Zimdahl, Phys. Rev. D **67**, 083513 (2003); L. Amendola and C. Quercellini, Phys. Rev. D **68**, 023514 (2003); M. B. Hoffman, arXiv:astro-ph/0307350; H. Ziaeepour, M. Axenides and K. Dimopoulos, JCAP **0407** (2004) 010; U. Franca and R. Rosenfeld, Phys. Rev. D **69**, 063517 (2004); A. V. Maccio *et al.*, Phys. Rev. D **69**, 123516 (2004); G. Huey and B. D. Wandelt, arXiv:astro-ph/0407196;

[4] Malik K A and Wands D 2009 *Phys. Rep.* **475** 1;

[5] E. J. Copeland, M. Sami, S. Tsujikawa, *Int. J. Mod. Phys.* D **15** 1753-1936 (2006) (`arXiv:hep-th/0603057`); V. Sahni, *Lect.Notes Phys.* **653** (2004) 141-180, (LANL preprint `astro-ph/0403324v3`);

[6] Spergel D N *et al* 2006 [WMAP Collaboration], arXiv:astro-ph/0603449.

[7] Olivares G Atrio–Barandela F and Pavón D 2005 *Phys. Rev.* D **71** 063523;.

[8] Olivares G Atrio–Barandela F and Pavón D 2006 *Phys. Rev.* D 74 043521;

[9] Olivares G Atrio–Barandela F and Pavón D 2008 *Phys. Rev.* D 77 063513;

[10] Valiviita J Majerotto E and Maartens R 2008 *JCAP* **0807** 020;

[11] Gavela M B Hernández D López Honórez L Mena O and Rigolin S 2009 JCAP **0907** 034.

[12] C. Clarkson, G. Ellis, J. Larena, and O. Umeh, Rep. Prog. Phys. 74, 112901 (2011).

[13] Hidalgo J C Christopherson A J and Malik K A 2013 *JCAP* 08 026

[14] Lema"tre G 1997 *Gen. Relativ. Gravit.* **29** 641 (English translation with historical comments); Tolman R C 1997 *Gen. Relativ. Gravit.* **29** 935 (Reprint with historical comments); Bondi H 1999 *Gen. Relativ. Gravit.* **31** 1783 (Reprinted with historical introduction);

[15] Krasiński A 1997 *Inhomogeneous Cosmological Models*, Cambridge University Press.

[16] Plebanski J and Krasinski A 2006 *An Introduction to General Relativity and Cosmology*, Cambridge University Press.

[17] K. Bolejko, A. Krasiński, C. Hellaby, M.-N. Célérier 2009, *Structures in the Universe by exact methods: formation, evolution, interactions* Cambridge University Press, Cambridge

[18] Bolejko K Celerier M N and Krasinski A 2011 *Class Quant Grav* **28** 164002

[19] Sussman R A 2010 *Gen Rel Grav* **42** 2813–2864 (*Preprint* `arXiv:1002.0173 [gr-qc]`)

[20] Sussman R A 2010 *Class.Quant.Grav.* **27** 175001 (*Preprint* `arXiv:1005.0717 [gr-qc]`)

[21] Sussman R A 2013 Class. and Quantum Grav. 30 065015;

[22] Sussman R A 2013 Class. and Quantum Grav. 30 065016

[23] Sussman R A 2008 *Class. Quantum Grav.* **25** 015012;

[24] Sussman R A 2013 *Class Quantum Grav* **30** 235001;

[25] Sussman R A and Izquierdo G 2011 Class. and Quantum Grav. 28 045006;

[26] Sussman R A Hidalgo J C Dunsby P K S and Germán G 2015 Physical Review D91, 063512;

[27] Sussman R A Quirós I and Martín González Osmel 2005 *Gen. Rel. Gravit.* **37** 2117

[28] Sussman R A 2008 *AIP Conf.Proc.* **1083** 228.

[29] Sussman R A 2009 *Phys Rev* D **79** 025009.

[30] German Izquierdo, Roberto C Blanquet-Jaramillo, Roberto A. Sussman, 2017 European Physical Journal C 78(3)

[31] German Izquierdo, Roberto C. Blanquet-Jaramillo, Roberto A. Sussman 2017 General Relativity and Gravitation 50(1)

[32] Sussman R A 2009 *Phys. Rev.* D **79** 025009. *Preprint* `arXiv:0801.3324`

[33] Pavón D. and Wang B., Gen. Relativ. Grav. **41**, 1 (2009).

[34] Wang B Atrio–Barandela F Abdalla E and Pavón D 2016 *Reports Progress on Physics* **79** 096901.

[35] T. Padmanabhan, *Structure formation in the universe*. Cambridge University Press (1993).

[36] Gunn J. E. and Gott III, .J. R. ApJ, 176:1, (1972).

[37] Mo H., van den Bosch F. C. , and White S *Galaxy Formation and Evolution*. Cambridge University Press (2010).

Capítulo 5

Discusión y conclusiones

Es importante comparar los resultados del presente trabajo con otros previos sobre la dinámica de los modelos LTB descritos por ecuaciones de evolución para los escalares cuasi–locales para diferentes mezclas de fuentes materia oscura fría y energía oscura acopladas. En [4], la mezcla que se consideró consistía en dos fluidos acoplados por un término de interacción $J_q = 3\alpha\mathcal{H}_q\rho_{mq}$, lo que lleva a un sistema dinámico autónomo de cinco dimensiones con la proyección homogénea definida por las funciones $\hat{\Omega}_m$ y $\hat{\Omega}_e$ y la proyección no homogénea definida por $\delta^{(m)}$, $\delta^{(e)}$ y $\delta^{(\mathcal{H})}$. En [10], consideramos las mismas fuentes y un término de acoplamiento dado por $J_q = 3\alpha\mathcal{H}_q\rho_{eq}$, con la adición de un fluido de radiación en la proyección homogénea (dominante cerca de la singularidad inicial) examinado en un apéndice.

En este trabajo, consideramos un término adicional de materia no relativista (materia bariónica) que es consistente con las observaciones cosmológicas y el término de acoplamiento es más general: $J_q = 3\alpha\mathcal{H}_q(\rho_{mq}+\rho_{eq})$. Como consecuencia, la proyección homogénea correspondiente ahora es tridimensional ($\hat{\Omega}_b$, $\hat{\Omega}_m$ y $\hat{\Omega}_e$) y la proyección no homogénea tiene una función adicional $\delta^{(B)}$. La adición de la fuente de materia bariónica hace más complejo

el estudio de sistemas dinámicos, especialmente la proyección no homogénea.

Podemos comparar la proyección homogénea de este trabajo con las de trabajos anteriores, ya que surgen algunas similitudes.

Por un lado, vemos que las proyecciones homogéneas en los tres trabajos contienen un atractor futuro similar, cuya posición está determinada por el tipo de interacción considerada, así como por los parámetros libres w y α (el atractor futuro tiene coordenadas: $\hat{\Omega}_m = 0, \hat{\Omega}_e = 1$ en [4], $\hat{\Omega}_m = -\alpha/w, \hat{\Omega}_e = 1 + \alpha/w$ en [10] y $\hat{\Omega}_b = 0, \hat{\Omega}_m = (1-\Delta)/2, \hat{\Omega}_e = (1+\Delta)/2$ con $\Delta^2 = 1 + 4\alpha/w$ en este trabajo).

Por otro lado, el atractor pasado tanto en [4] como en [10] (con coordenadas $\hat{\Omega}_m = 1 + \alpha/w, \hat{\Omega}_e = -\alpha/w$ y $\hat{\Omega}_m = 1, \hat{\Omega}_e = 0$ respectivamente) se puede relacionar fácilmente con el punto crítico $P2$ en el presente trabajo ($\hat{\Omega}_b = 0, \hat{\Omega}_m = (1+\Delta)/2, \hat{\Omega}_e = (1-\Delta)/2$).

Nótese que, mientras que $P2$ es un punto silla, se comporta como un atractor pasado en el subespacio $\hat{\Omega}_m - -\hat{\Omega}_e$ (generado por los vectores propios con valores propios definidos positivos), mientras que actúa como un atractor futuro en la dirección paralela al eje $\hat{\Omega}_b$ (ver el artículo). Podemos concluir que el atractor pasado (cuya posición depende de la interacción y los parámetros libres considerados) de los trabajos anteriores cambió a un punto silla cuando se añade una fuente extra de materia bariónica. De hecho, en este trabajo se añade un nuevo atractor pasado $P3$, que puede jugar un papel interesante en la evolución de los perfiles iniciales (ver el artículo).

Se encontró una línea invariante de la proyección homogénea en [10], conectando el origen del plano $\hat{\Omega}_m - -\hat{\Omega}_e$ con el atractor futuro. En [4], también encontramos una línea invariante que conecta el punto $\hat{\Omega}_m = 0, \hat{\Omega}_e = 0$ y el atractor pasado. Dado que ninguna trayectoria del espacio de fases puede cruzar esta última línea invariante, algunas

condiciones iniciales, cerca del atractor pasado (y debajo de esta línea) terminarían su evolución hacia el eje $\hat{\Omega}_e = 0$ (ver figura 1 en [4]). Mirando la proyección $\hat{\Omega}_b = 0$ en el presente trabajo, vemos que ni la línea que conecta el origen con el punto de silla $P2$ ni la línea que conecta el origen con el atractor futuro son subespacios invariantes. De hecho, no se pueden definir otros subespacios invariantes de interés para la interacción $J_q = 3\alpha\mathcal{H}_q(\rho_{mq} + \rho_{eq})$ en la proyección tridimensional homogénea. Aunque todavía puede haber trayectorias que evolucionen hacia el eje $\hat{\Omega}_e = 0$ en este trabajo, están relacionadas con la proyección $\hat{\Omega}_b = 0$ y pueden evitarse en un escenario cosmológico considerando una fuente extra de materia bariónica.

Para definir la función Γ en [4] y [10], se encontraron soluciones analíticas para ρ_{mq} y ρ_{eq} en términos del factor de escala L. En [4] y debido a la elección de la interacción, la función ρ_{mq} era particularmente simple como $\rho_{mq} = \rho_{mq0}L^{-3(1-\alpha)}$, permitiéndonos conectar la función Γ directamente a $\delta^{(m)}$. Por otro lado, en [10], era ρ_{eq} el que tenía una dependencia de ley de potencia en L como $\rho_{eq} = \rho_{eq0}L^{-3(1+w+\alpha)}$, lo que resultó en que Γ estuviera relacionado con $\delta^{(m)}$. En el presente trabajo, la interacción más general y la adición de la fuente de materia bariónica, encontramos una solución analítica para ρ_{mq} y ρ_{eq} en términos de L, pero no se encontró una ley de potencia simple obtenido para cualquiera de ellos, haciendo que la función Γ dependa de $\delta^{(B)}$, $\delta^{(m)}$ y $\delta^{(e)}$ (ver el artículo).

Finalmente, vale la pena considerar la adición de una fuente similar a la radiación casi homogénea al sistema dinámico, procediendo de manera similar a como lo hicimos en el apéndice en [10]. Tal fuente de radiación produciría una nueva función Ω_r que se agregaría al conjunto de variables del espacio de fases (con $\delta_r = 0$, ya que sería una radiación homogéneamente distribuida en el universo), lo que conduciría a una proyección

homogénea de cuatro dimensiones. Es natural suponer que el punto crítico $P3$ (relacionado con un modelo sin fuentes de materia oscura fría o energía oscura) ya no sería un atractor del sistema, ya que aparecería un nuevo atractor en el valor $\Omega_r = 1$, con el resto de las funciones $\Omega = 0$. Este atractor se entiende fácilmente dada la evolución con el factor de escala L de los escalares cuasi–locales. Los escalares cuasi–locales ρ_{bq}, ρ_{mq} y ρ_{eq} seguirían evolucionando con L como una ley de potencias), mientras que $\rho_{rq} = \rho_{rq0}L^{-4}$. Como $L \to 0$ para cada capa, la fuente de radiación dominaría la expansión temprana cerca de la singularidad inicial de la misma manera que en [10].

Como comentario final, la adición de la fuente bariónica y la consideración de un término de acoplamiento más general en este trabajo agregaron más complejidad al análisis del sistema dinámico, pero aún es posible obtener información interesante y obtener soluciones numéricas similares a los anteriores trabajos.

Hemos generalizado en el presente trabajo los resultados de trabajos anteriores [4, 10] al estudiar la dinámica de las soluciones LTB que contienen tres fuentes: materia bariónica con materia oscura fría y energía oscura acopladas interactivamente. El término de acoplamiento que consideramos es una generalización razonable de los utilizados en los artículos anteriores, ya que es proporcional a la suma de las densidades de energía de ambas fuentes oscuras (no solo a una de ellas). Usando el formalismo de los escalares cuasi–locales, transformamos las ecuaciones de evolución de Einstein en un sistema dinámico autónomo de 7 dimensiones. El sistema dinámico se puede descomponer en dos subsistemas: el subsistema homogéneo invariante tridimensional cuyas variables son los escalares cuasi–locales adimensionales $(\hat{\Omega}_b, \hat{\Omega}_m, \hat{\Omega}_e)$, relacionados con el modelo FLRW, y un subespacio de 4 dimensiones para las funciones δ $(\delta^{(B)}, \delta^{(m)}, \delta^{(e)}, \delta^{(\mathcal{H})})$ que pueden interpretarse como

desviaciones exactas de la métrica FLRW.

Para la proyección homogénea obtuvimos cuatro puntos críticos resumidos en la tabla (ver el artículo): un punto silla $P1$, un atractor futuro $P2$, un atractor pasado $P3$ y un punto silla $P4$. El comportamiento de los puntos críticos se examinó bajo el supuesto de que w es de orden/inferior a -1 y $0 < \alpha < 0.25$, con base en los límites observacionales que se han obtenido para este acoplamiento en la cosmología FLRW [2, 3, 11, 12]. Las funciones δ se calculan con un conjunto de condiciones iniciales para evitar singularidades de cruce de capa (instante para el cual $\Gamma \to 0$, con Γ definido en el artículo). Tener $\Gamma > 0$ es una condición necesaria para evitar singularidades de cruce de capas para las cuales $\delta^{(B)}, \delta^{(m)}, \delta^{(e)}, \delta^{(\mathcal{H})}$ divergen en tiempos finitos de evolución.

Finalmente, para ilustrar cómo resolver numéricamente las ecuaciones de evolución, consideramos un ejemplo específico de un conjunto dado de perfiles iniciales (ver el artículo), con partición de capas para la coordenada r y parámetros libres ($w = -1$ y $\alpha = 0.1$). En este ejemplo, dos capas internas (r_1 y r_2) evolucionaron con $\hat{\Omega}_b, \hat{\Omega}_m, \hat{\Omega}_e$ tendiendo a infinito en un tiempo finito mientras que las capas externas evolucionan hacia el atractor futuro (ver figura 1 del artículo). Como no hay cruce de capas durante la evolución (ver figura 2 del artículo), podemos concluir que $\hat{\Omega}_b, \hat{\Omega}_m, \hat{\Omega}_e$ que diverge para las capas internas corresponde a una expansión máxima o instante en el que $\mathcal{H}_q = 0$ marca el inicio de un escenario de colapso. Debido a que los modelos LTB no son homogéneos, estos instantes ocurren en diferentes tiempos cósmicos para diferentes observadores comóviles, aunque es posible caracterizar estos tiempos como un solo tiempo calculando numéricamente (caso por caso) el $\langle t_{\max} \rangle$ promedio (ver figura 3 del artículo). De esta manera, podemos relacionar este cálculo numérico con el tiempo de colapso en un perfil del tipo "top hat"de los

modelos de perturbaciones esféricas discutidos en la literatura.

Bibliografía

[1] P. A. R. Ade, et al., arXiv:1303.5076v1 (2013);

[2] Olivares G Atrio–Barandela F and Pavón D 2005 *Phys. Rev.* D **71** 063523;

[3] Olivares G Atrio–Barandela F and Pavón D 2006 *Phys. Rev.* D 74 043521;

[4] German Izquierdo, Roberto C. Blanquet-Jaramillo, Roberto A. Sussman 2017 General Relativity and Gravitation 50(1);

[5] Sussman R A and Izquierdo G 2011 Class. and Quantum Grav. 28 045006;

[6] Sussman R A 2009 *Phys Rev* D **79** 025009;

[7] Sussman R A 2013 *Class Quantum Grav* **30** 235001;

[8] Sussman R A Hidalgo J C Dunsby P K S and Germán G 2015 Physical Review D91, 063512;

[9] Sussman R A 2008 *AIP Conf.Proc.* **1083** 228;

[10] German Izquierdo, Roberto C Blanquet-Jaramillo, Roberto A. Sussman, 2017 European Physical Journal C 78(3)

[11] Olivares G Atrio–Barandela F and Pavón D 2008 *Phys. Rev.* D 77 063513;

[12] Wang B Atrio–Barandela F Abdalla E and Pavón D 2016 *Reports Progress on Physics* **79** 096901.